tumor efficacy.

Accumulation and activation state of immune cells in tumor treated with the combination of gp100/DC-immunization and chemokine-expressing AdRGD injection

B16BL6 tumors were harvested 2 days after intratumoral injection of chemokine-expressing AdRGD (Protocol-2) and were analyzed for the levels of infiltrating T cells by immunohistochemical staining. As shown in Figure 7, tumors injected with AdRGD-CCL17, -CCL22, or -CCL27 exhibited enhanced $CD3^+$ T-cell accumulation, whereas the number of T cells in tumor tissue was only slightly elevated by injection of AdRGD-CCL19, -CCL20, or -CCL21, and did not change between the AdRGD-XCL1- or AdRGD-CX3CL1-injected group and the AdRGD-Luc-injected group. These data disagreed with the observation that intratumoral injection of AdRGD-CCL19 could attract a large number of T cells in mice without gp100/DC-immunization as shown in Figures 3h and 4a, suggesting that responsiveness of T cells for chemokines was altered by the activation state of the host's immune system, that is, sensitization of T cells by gp100/DC-administration. Importantly, the levels of tumor-infiltrating T cells showed positive correlation for antitumor efficacy (Figure 6) in mice treated with gp100/DC immunization and each chemokine-expressing AdRGD injection. Because the number of infiltrating NK cells and DCs was low in tumors injected with any AdRGD in this combinational protocol as well as in Protocol-1 (data not shown), we theorized that infiltrating CTLs were the major effector cells responsible for improved anti-B16BL6 tumor effects.

In order to evaluate the activation state of tumor-associated CTLs, we performed RT-PCR analysis specific for perforin, granzyme B, and IFN-γ, which are the major cytotoxic molecules and secreted cytokines in activated CTLs (Figure 8). We focused on tumors treated with AdRGD-CCL17 and AdRGD-CCL19, which induced the most effective T-cell infiltration in Protocol-2 and -1, respectively. The combination with gp100/DC-immunization notwithstanding, PCR products derived from transcripts of perforin, granzyme B, or IFN-γ were detected at higher levels in tumors injected with AdRGD-CCL17 or AdRGD-CCL19 as compared with AdRGD-Luc-injected tumors. In the absence of gp100/DC immunization, AdRGD-CCL19-injected tumors expressed more perforin- and granzyme B-specific mRNA than AdRGD-CCL17-injected tumors, whereas intratumoral injection of AdRGD-CCL17 in combination with gp100/DC immunization induced higher perforin, granzyme B, and IFN-γ mRNA expression in tumor tissue than AdRGD-

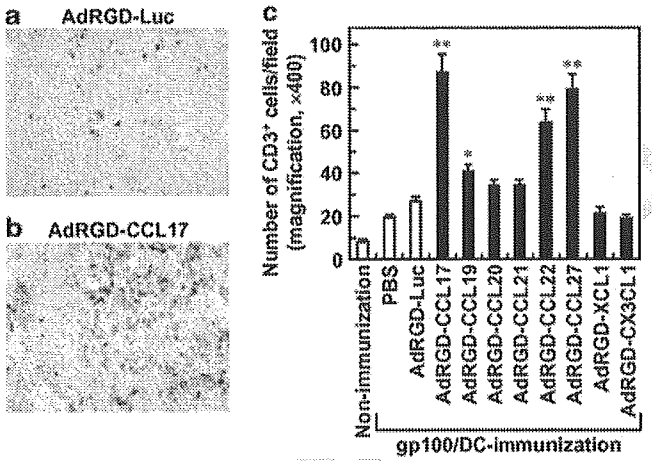

Figure 7 Infiltration of T cells into B16BL6 tumors of mice treated with the combination of gp100/DC-immunization and intratumoral injection of chemokine-expressing AdRGD. B16BL6 cells were intradermally inoculated into the right flank of C57BL/6 mice at 4×10^5 cells/mouse. The next day, the mice were intradermally injected with 10^6 gp100/DCs in the left flank. Then, the tumors (5–7 mm in diameter) were injected with each chemokine-expressing AdRGD or AdRGD-Luc at 3×10^8 PFU. Likewise, PBS was administered into control tumors. On day 2 after intratumoral injection, immunohistochemical staining against CD3 for determining T cells was performed with frozen tumor sections. (**a** and **b**) Original magnifications are $\times 200$. (**c**) The number of CD3-positive cells in the intratumoral section was assessed by counting six fields per specimen under $\times 400$ magnification. The data represent the mean$\pm$s.e. of results from three tumors. Statistical analysis was carried out by Welch's *t*-test: $^*P<0.01$, $^{**}P<0.001$ versus AdRGD-Luc-injected group.

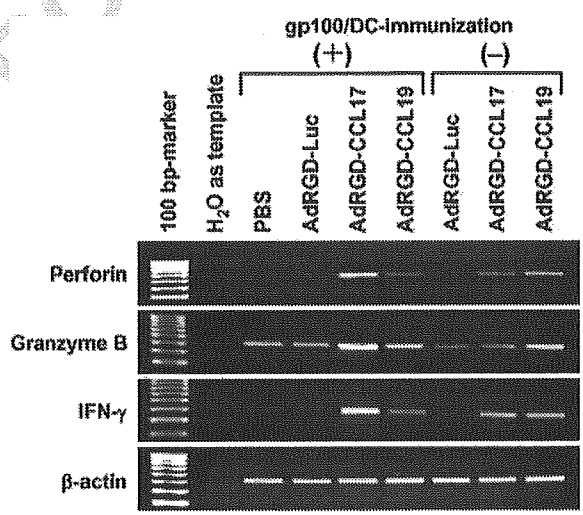

Figure 8 Activation state of infiltrating immune cells in B16BL6 tumors injected intratumorally with chemokine-expressing AdRGD in combination with or without gp100/DC-immunization. B16BL6 cells were intradermally inoculated into the right flank of C57BL/6 mice at 4×10^5 cells/mouse. After 1 day, the mice were intradermally injected with (Protocol-2) or without (Protocol-1) 10^6 gp100/DCs in the left flank. The tumor (5–7 mm in diameter) in Protocol-1 or -2 was injected with AdRGD-CCL17, AdRGD-CCL19, or AdRGD-Luc at 3×10^8 PFU. Likewise, PBS was administered into control tumors. After 2 days, total RNA was isolated from the tumors collected from these mice, and then RT-PCR, specific for perforin, granzyme B, and IFN-γ transcripts, was performed as described in the Materials and methods section. The PCR products were electrophoresed through a 3% agarose gel, stained with ethidium bromide, and visualized under ultraviolet light.

CCL19 injection. In addition, expression levels of perforin, granzyme B, and IFN-γ mRNA were increased in AdRGD-CCL17-injected groups by receiving gp100/DC immunization. On the other hand, gp100/DC immunization of AdRGD-CCL19-injected groups tended to decrease or did not alter mRNA expression levels of these three activation markers. Though intratumoral injection with AdRGD-CCL19 in protocol-1 was able to induce T-cell infiltration much more efficiently than AdRGD-CCL17 injection in protocol-2 (Figures 4a and 7c), RT-PCR analysis revealed that AdRGD-CCL17-injected tumor in gp100/DC-immunized mice contained activated T cells in higher frequency as compared with tumor treated with AdRGD-CCL19 injection alone. These results correlate closely with differences in the antitumor effects (Figures 1 and 6), strongly suggesting that efficient accumulation of activated tumor-specific CTLs at a local tumor site is a key factor for establishment of efficacious cancer immunotherapy.

Discussion

Investigations of the relationship between the prognosis and the infiltration frequency of tumor-associated immune cells in patients with cancer have indicated that post-treatment recurrence or metastasis is significantly suppressed in cases that exhibit high immune cell-infiltration in primary tumor tissue,[34–36] and it is widely believed that T cells represent the most potent antitumor effector cells.[37–39] Therefore, the establishment of immunotherapy capable of promoting tumor cell–immune cell interaction is considered critical for improving the cure rate for cancer. Based on these results, an approach that attempts to reinforce immune cell accumulation in tumor tissue by applying chemokines, which control migration and infiltration of immune cells into the local site, is very attractive for the development of efficacious cancer immunotherapy. We previously demonstrated that tumor cells transduced with AdRGD encoding chemokine genes could produce and secrete chemokines that exhibit original bioactivity, and that inoculation with chemokine gene-transfected tumor cells was very useful for screening antitumor effects based on facilitation of chemokine secretion in tumor tissue.[25,26] In the present study, in order to evaluate the potential of chemokine-based immunogenetherapy for cancer by using an AdRGD system capable of efficient gene transduction in various tumors, we examined antitumor efficacy and accumulation of tumor-associated immune cells in mice directly injected with chemokine-expressing AdRGD into established tumor tissue.

An established murine B16BL6 melanoma injected with AdRGD-CCL17, -CCL19, -CCL20, -CCL21, -CCL22, -CCL27, -XCL1, or -CX3CL1 exhibited slightly delayed growth compared with control vector-injected tumor. Moreover, immunohistochemical analysis of these tumors demonstrated that intratumoral injection of AdRGD-CCL19 could significantly induce both $CD4^+$ and $CD8^+$ T-cell infiltration in parenchyma of tumor tissue, and that AdRGD-CCL17 injection was superior in promoting NK cell accumulation at the peritumoral site. Generally, the infiltration of immune cells rarely occurs in newly formed vessels in solid tumor, and immune cells that penetrate from existing blood vessels, which are present around tumor tissue, arrive at and accumulate in tumor parenchyma through the tumor border region.[40] This explains our observation that NK cells accumulated in the tumor peripheral zone, but did not infiltrate the tumor parenchyma upon intratumoral injection of chemokine-expressing AdRGD. On the other hand, we speculated that T-cell infiltration occurred directly from tumor vessels in the AdRGD-CCL19-treated group, because a large number of T cells were observed in the center of tumor tissue as well as near the border. This theory is supported by a previous report that CCL19 could increase the expression of cell adhesion molecules on vascular endothelial cells.[41] Although CCL19 and CCL21 are ligand for an identical chemokine receptor (CCR7), the level of T-cell infiltration in AdRGD-CCL21-injected tumors was obviously lower than that in AdRGD-CCL19-injected tumors. Similarly, regarding CCL17 and CCL22, which shared CCR4 as their receptor, the number of NK cells at periphery of AdRGD-CCL22-injected tumors was half of that of AdRGD-CCL17-injected tumors. Because chemokines are heparin/heparan sulfate-binding proteins and this property modulates their activity, diffusion, and stability in tissue, we speculated that an affinity to heparin/heparan sulfate of each chemokine might determine the difference of immune cell infiltration between CCL19- and CCL21-transduced tumors or between CCL17- and CCL22-transduced tumors. Previous studies have shown that intratumoral injections of CCL20 and CCL21 induce a large accumulation of mature DCs related with strong antitumor responses.[42,43] However, we did not detect significant increase of infiltrating $CD11c^+$ DCs in B16BL6 tumors injected with any chemokine-expressing AdRGDs including AdRGD-CCL20 and -CCL21. We speculated that the disagreement between our observation and the results in previous studies was caused by a difference of the tumor model which was examined. Therefore, in order to select appropriate chemokine for intratumoral gene transduction to augment tumor-infiltrating immune cells efficiently, we need to consider not only its receptor-specificity but also its *in vivo* characteristics and variety of tumors. However, we could not recognize a correlation between tumor suppressive effect and the number of tumor-infiltrating immune cells in mice treated with each chemokine-expressing AdRGD. Because most immune cells that infiltrated into tumors with injection of chemokine-expressing AdRGD were perforin-negative, that is, in naive status, combinational therapy that included another treatment, which could prime and activate immune effector cells, would be required for achievement of more potent antitumor efficacy.

We previously succeeded in efficiently transducing genes into DCs by applying the AdRGD system rather than a conventional vector,[28,44] and demonstrated that

DCs transduced with the TAA gene using AdRGD are effective vaccine carriers that induce tumor-specific immune responses in mice.[33,45] Thus, we evaluated the antitumor effect in mice of intratumoral injection of chemokine-expressing AdRGD combined with intradermal immunization of DCs transduced with gp100 by AdRGD. Lytic activity of B16BL6-specific CTLs in splenocytes from B16BL6 tumor-bearing mice was considerably enhanced by single gp100/DC-immunization, indicating that administration of TAA/DCs could promote initiation and amplification of tumor immunity in individuals that exhibited ongoing tumor growth (therapeutic protocol) as well as in intact mice (vaccine protocol). In combination with gp100/DC-immunization, intratumoral injection with AdRGD-CCL17, -CCL22, or -CCL27 markedly suppressed B16BL6 tumor growth in mice. In addition, immunohistochemical analysis and RT-PCR analysis using RNA isolated from treated tumors revealed that CCL17-, CCL22-, or CCL27-gene transduction induced efficient accumulation of activated T cells in tumor tissue. CCL19, on the other hand, only slightly induced activated T-cell accumulation in tumors of gp100/DC-immunized mice, whereas naive T cells were dramatically attracted to tumors injected with AdRGD-CCL19 alone. These conflicting results can be explained by the evidence that CCR7, which is the corresponding receptor for CCL19, is expressed on naive T cells, but not on effector-type T cells.[46] Kim *et al.* demonstrated that DC-stimulation led naive T cells to downregulation of lymphoid tissue homing related CCR7 and CXCR5, and upregulation of Th1/2 effector tissue-targeting chemoattractant receptors such as CCR4 (receptor for CCL17 and CCL22), CCR5, CXCR6, and CRTH2.[47] In addition, Mullins *et al.* reported that coexpression of CCR4 and CXCR3 by activated $CD8^+$ T cells derived from the peripheral blood or tumor-involved lymph nodes of patients with stage III metastatic melanoma was significantly associated with enhanced survival.[48] CCR10 (receptor for CCL27) is known as a chemokine receptor that is preferentially expressed among blood leukocytes by a subset of memory $CD4^+$ and $CD8^+$ T cells, and CCR10-positive T cells that coexpress the skin-homing receptor, cutaneous lymphocyte antigen, can act as both 'central' and 'effector' memory T cells.[49] These previous results supported our data that intratumoral injection of AdRGD-CCL17, -CCL22, or -CCL27, but not AdRGD-CCL19, was effective for promoting the anti-B16BL6 tumor efficacy and the infiltration of immune effector cells in mice immunized with gp100/DCs. Therefore, the selection of chemokine in cancer immunogenetherapy must consider the host's immune activation status and characteristics of other combined therapies on immunomodulation.

In conclusion, our results revealed that chemokine gene transduction into established tumors using AdRGD could enhance accumulation of immune cells, and would greatly contribute to the development of efficacious cancer immunogenetherapy based on 'Immune Cell Delivery System'. Additionally, combinational therapy that included immunization with TAA-delivered DCs and intratumoral injection of chemokine-expressing AdRGD, such as AdRGD-CCL17, -CCL22, and -CCL27, could more effectively suppress tumor growth as compared with each treatment alone, indicating that the combined treatment, which can systemically induce tumor-specific effector T cells, is a promising strategy for potentiating antitumor efficacy and tumor-infiltrating effector cells by direct injection of chemokine-expressing vector into tumors. Now, in order to apply our chemokine gene-based cancer immunotherapy to not only primary tumors but also metastatic tumors in which intratumoral injection of vectors is physically difficult, we are pushing forward development of transductionally and transcriptionally tumor-targeting vector, which can specifically deliver a chemokine gene into tumor cells by systemic administration.[50,51]

Abbreviations

AdRGD, RGD fiber-mutant adenoviral vector; CTL, cytotoxic T lymphocyte; DC, dendritic cell; FBS, fetal bovine serum; HE, hematoxylin and eosin; IFN, interferon; mAb, monoclonal antibody; NK, natural killer; PBS, phosphate-buffered saline; PFU, plaque-forming unit; RT-PCR, reverse transcription-polymerase chain reaction; TAA, tumor-associated antigen; Th, helper T cell.

Acknowledgements

We are grateful to Drs Osamu Yoshie and Takashi Nakayama (Department of Microbiology, Kinki University School of Medicine, Osaka-Sayama, Japan) for providing plasmids containing murine chemokine cDNA, to Yoshinobu Kimura (Department of Biopharmaceutics, Kyoto Pharmaceutical University, Kyoto, Japan) for technical assistance, and to KIRIN Brewery Co., Ltd (Tokyo, Japan) for providing recombinant murine granulocyte/macrophage colony-stimulating factor. The present study was supported in part by the Research on Health Sciences focusing on Drug Innovation from The Japan Health Sciences Foundation; by grants from the Bioventure Development Program of the Ministry of Education, Culture, Sports, Science and Technology of Japan, and by grants from the Ministry of Health, Labour and Welfare in Japan.

References

1 Urban JL, Schreiber H. Tumor antigens. *Annu Rev Immunol* 1992; **10**: 617–644.
2 Mackensen A, Carcelain G, Viel S *et al.* Direct evidence to support the immunosurveillance concept in a human regressive melanoma. *J Clin Invest* 1994; **93**: 1397–1402.
3 Smyth MJ, Godfrey DI, Trapani JA. A fresh look at tumor immunosurveillance and immunotherapy. *Nat Immunol* 2001; **2**: 293–299.

Q1

4 Tada T, Ohzeki S, Utsumi K *et al.* Transforming growth factor-β-induced inhibition of T cell function. Susceptibility difference in T cells of various phenotypes and functions and its relevance to immunosuppression in the tumor-bearing state. *J Immunol* 1991; **146**: 1077–1082.
5 Ohm JE, Carbone DP. VEGF as a mediator of tumor-associated immunodeficiency. *Immunol Res* 2001; **23**: 263–272.
6 Jacobs SK, Wilson DJ, Kornblith PL, Grimm EA. Interleukin-2 or autologous lymphokine-activated killer cell treatment of malignant glioma: phase I trial. *Cancer Res* 1986; **46**: 2101–2104.
7 Rosenberg SA, Yannelli JR, Yang JC *et al.* Treatment of patients with metastatic melanoma with autologous tumor-infiltrating lymphocytes and interleukin 2. *J Natl Cancer Inst* 1994; **86**: 1159–1166.
8 Mandelboim O, Vadai E, Fridkin M *et al.* Regression of established murine carcinoma metastases following vaccination with tumour-associated antigen peptides. *Nat Med* 1995; **1**: 1179–1183.
9 Conry RM, Curiel DT, Strong TV *et al.* Safety and immunogenicity of a DNA vaccine encoding carcinoembryonic antigen and hepatitis B surface antigen in colorectal carcinoma patients. *Clin Cancer Res* 2002; **8**: 2782–2787.
10 Dranoff G, Jaffee E, Lazenby A *et al.* Vaccination with irradiated tumor cells engineered to secrete granulocyte-macrophage colony-stimulating factor stimulates potent, specific, and long-lasting anti-tumor immunity. *Proc Natl Acad Sci USA* 1993; **90**: 3539–3543.
11 Asada H, Kishida T, Hirai H *et al.* Significant antitumor effects obtained by autologous tumor cell vaccine engineered to secrete interleukin (IL)-12 and IL-18 by means of the EBV/lipoplex. *Mol Ther* 2002; **5**: 609–616.
12 Mayordomo JI, Zorina T, Storkus WJ *et al.* Bone marrow-derived dendritic cells pulsed with synthetic tumour peptides elicit protective and therapeutic antitumour immunity. *Nat Med* 1995; **1**: 1297–1302.
13 Song W, Kong HL, Carpenter H *et al.* Dendritic cells genetically modified with an adenovirus vector encoding the cDNA for a model antigen induce protective and therapeutic antitumor immunity. *J Exp Med* 1997; **186**: 1247–1256.
14 Nair SK, Heiser A, Boczkowski D *et al.* Induction of cytotoxic T cell responses and tumor immunity against unrelated tumors using telomerase reverse transcriptase RNA transfected dendritic cells. *Nat Med* 2000; **6**: 1011–1017.
15 Yoshie O, Imai T, Nomiyama H. Chemokines in immunity. *Adv Immunol* 2001; **78**: 57–110.
16 Zlotnik A, Yoshie O. Chemokines: a new classification system and their role in immunity. *Immunity* 2000; **12**: 121–127.
17 Murphy PM. The molecular biology of leukocyte chemoattractant receptors. *Annu Rev Immunol* 1994; **12**: 593–633.
18 Bokoch GM. Chemoattractant signaling and leukocyte activation. *Blood* 1995; **86**: 1649–1660.
19 Homey B, Muller A, Zlotnik A. Chemokines: agents for the immunotherapy of cancer? *Nat Rev Immunol* 2002; **2**: 175–184.
20 Sharma S, Stolina M, Luo J *et al.* Secondary lymphoid tissue chemokine mediates T cell-dependent antitumor responses *in vivo*. *J Immunol* 2000; **164**: 4558–4563.
21 Fushimi T, Kojima A, Moore MA, Crystal RG. Macrophage inflammatory protein 3α transgene attracts dendritic cells to established murine tumors and suppresses tumor growth. *J Clin Invest* 2000; **105**: 1383–1393.
22 Braun SE, Chen K, Foster RG *et al.* The CC chemokine CKβ-11/MIP-3β/ELC/Exodus 3 mediates tumor rejection of murine breast cancer cells through NK cells. *J Immunol* 2000; **164**: 4025–4031.
23 Miyata T, Yamamoto S, Sakamoto K, Morishita R, Kaneda Y. Novel immunotherapy for peritoneal dissemination of murine colon cancer with macrophage inflammatory protein-1β mediated by a tumor-specific vector, HVJ cationic liposomes. *Cancer Gene Ther* 2001; **8**: 852–860.
24 Guo J, Zhang M, Wang B *et al.* Fractalkine transgene induces T-cell-dependent antitumor immunity through chemoattraction and activation of dendritic cells. *Int J Cancer* 2003; **103**: 212–220.
25 Gao J-Q, Tsuda Y, Katayama K *et al.* Antitumor effect by interleukin-11 receptor α-locus chemokine/CCL27, introduced into tumor cells through a recombinant adenovirus vector. *Cancer Res* 2003; **63**: 4420–4425.
26 Okada N, Gao J-Q, Sasaki A *et al.* Anti-tumor activity of chemokine is affected by both kinds of tumors and the activation state of the host's immune system: implications for chemokine-based cancer immunotherapy. *Biochem Biophys Res Commun* 2004; **317**: 68–76.
27 Mizuguchi H, Koizumi N, Hosono T *et al.* A simplified system for constructing recombinant adenoviral vectors containing heterologous peptides in the HI loop of their fiber knob. *Gene Therapy* 2001; **8**: 730–735.
28 Okada N, Masunaga Y, Okada Y *et al.* Gene transduction efficiency and maturation status in mouse bone marrow-derived dendritic cells infected with conventional or RGD fiber-mutant adenovirus vectors. *Cancer Gene Ther* 2003; **10**: 421–431.
29 Mizuguchi H, Kay MA. Efficient construction of a recombinant adenovirus vector by an improved *in vitro* ligation method. *Hum Gene Ther* 1998; **9**: 2577–2583.
30 Mizuguchi H, Kay MA. A simple method for constructing E1- and E1/E4-deleted recombinant adenoviral vectors. *Hum Gene Ther* 1999; **10**: 2013–2017.
31 Lutz MB, Kukutsch N, Ogilvie AL *et al.* An advanced culture method for generating large quantities of highly pure dendritic cells from mouse bone marrow. *J Immunol Methods* 1999; **223**: 77–92.
32 Okada N, Tsujino M, Hagiwara Y *et al.* Administration route-dependent vaccine efficiency of murine dendritic cells pulsed with antigens. *Br J Cancer* 2001; **84**: 1564–1570.
33 Okada N, Masunaga Y, Okada Y *et al.* Dendritic cells transduced with gp100 gene by RGD fiber-mutant adenovirus vectors are highly efficacious in generating anti-B16BL6 melanoma immunity in mice. *Gene Therapy* 2003; **10**: 1891–1902.
34 Eerola AK, Soini Y, Paakko P. A high number of tumor-infiltrating lymphocytes are associated with a small tumor size, low tumor stage, and a favorable prognosis in operated small cell lung carcinoma. *Clin Cancer Res* 2000; **6**: 1875–1881.
35 Yin XY, Lu MD, Lai YR, Liang LJ, Huang JF. Prognostic significances of tumor-infiltrating S-100 positive dendritic cells and lymphocytes in patients with hepatocellular carcinoma. *Hepatogastroenterology* 2003; **50**: 1281–1284.
36 Fukunaga A, Miyamoto M, Cho Y *et al.* $CD8^+$ tumor-infiltrating lymphocytes together with $CD4^+$ tumor-infiltrating lymphocytes and dendritic cells improve the prognosis of patients with pancreatic adenocarcinoma. *Pancreas* 2004; **28**: e26–e31.

37 Naito Y, Saito K, Shiiba K *et al.* CD8$^+$ T cells infiltrated within cancer cell nests as a prognostic factor in human colorectal cancer. *Cancer Res* 1998; **58**: 3491–3494.
38 Shankaran V, Ikeda H, Bruce AT *et al.* IFN-γ and lymphocytes prevent primary tumour development and shape tumour immunogenicity. *Nature* 2001; **410**: 1107–1111.
39 Zhang L, Conejo-Garcia JR, Katsaros D *et al.* Intratumoral T cells, recurrence, and survival in epithelial ovarian cancer. *N Engl J Med* 2003; **348**: 203–213.
40 Smolle J, Hofmann-Wellenhof R, Fink-Puches R. Melanoma and stroma: an interaction of biological and prognostic importance. *Semin Cutan Med Surg* 1996; **15**: 326–335.
41 Luther SA, Bidgol A, Hargreaves DC *et al.* Differing activities of homeostatic chemokines CCL19, CCL21, and CXCL12 in lymphocyte and dendritic cell recruitment and lymphoid neogenesis. *J Immunol* 2002; **169**: 424–433.
42 Crittenden M, Gough M, Harrington K, Olivier K, Thompson J, Vile RG. Expression of inflammatory chemokines combined with local tumor destruction enhances tumor regression and long-term immunity. *Cancer Res* 2003; **63**: 5505–5512.
43 Sharma S, Stolina M, Luo J *et al.* Secondary lymphoid tissue chemokine mediates T cell-dependent antitumor responses *in vivo*. *J Immunol* 2000; **164**: 4558–4563.
44 Okada N, Tsukada Y, Nakagawa S *et al.* Efficient gene delivery into dendritic cells by fiber-mutant adenovirus vectors. *Biochem Biophys Res Commun* 2001; **282**: 173–179.
45 Okada N, Saito T, Masunaga Y *et al.* Efficient antigen gene transduction using Arg-Gly-Asp fiber-mutant adenovirus vectors can potentiate antitumor vaccine efficacy and maturation of murine dendritic cells. *Cancer Res* 2001; **61**: 7913–7919.
46 Moser B, Loetscher P. Lymphocyte traffic control by chemokines. *Nat Immunol* 2001; **2**: 123–128.
47 Kim CH, Nagata K, Butcher EC. Dendritic cells support sequential reprogramming of chemoattractant receptor profiles during naive to effector T cell differentiation. *J Immunol* 2003; **171**: 152–158.
48 Mullins IM, Slingluff CL, Lee JK *et al.* CXC chemokine receptor 3 expression by activated CD8$^+$ T cells is associated with survival in melanoma patients with stage III disease. *Cancer Res* 2004; **64**: 7697–7701.
49 Hudak S, Hagen M, Liu Y *et al.* Immune surveillance and effector functions of CCR10$^+$ skin homing T cells. *J Immunol* 2002; **169**: 1189–1196.
50 Koizumi N, Mizuguchi H, Sakurai F, Yamaguchi T, Watanabe Y, Hayakawa T. Reduction of natural adenovirus tropism to mouse liver by fiber-shaft exchange in combination with both CAR- and αv integrin-binding ablation. *J Virol* 2003; **77**: 13062–13072.
51 Okada Y, Okada N, Mizuguchi H, Hayakawa T, Nakagawa S, Mayumi T. Transcriptional targeting of RGD fiber-mutant adenovirus vectors can improve the safety of suicide gene therapy for murine melanoma. *Cancer Gene Ther* 2005; **12**: 608–616.

NPG.CGT.7700903

doi:10.1016/j.ymthe.2005.10.007

ARTICLE

Quantitative Comparison of Intracellular Trafficking and Nuclear Transcription between Adenoviral and Lipoplex Systems

Susumu Hama,[1,2] Hidetaka Akita,[1,2] Rie Ito,[1] Hiroyuki Mizuguchi,[3] Takao Hayakawa,[4] and Hideyoshi Harashima[1,2,*]

[1]*Graduate School of Pharmaceutical Sciences, Hokkaido University, Sapporo, Hokkaido 060-0812, Japan*
[2]*CREST, Japan Science and Technology Corporation, Tokyo, Japan*
[3]*Laboratory of Gene Transfer and Regulation, National Institute of Biomedical Innovation, Osaka 567-0085, Japan*
[4]*Pharmaceuticals and Medical Devices Agency, Tokyo 100-0013, Japan*

**To whom correspondence and reprint requests should be addressed. Fax: +81 11 706 4879. E-mail: harasima@pharm.hokudai.ac.jp.*

To develop nonviral gene vectors that are sufficient for clinical application, it is necessary to understand why and to what extent nonviral vectors are inferior to viral vectors, which in general show a more efficient transfection activity. This study describes a systematic and quantitative comparison of the cellular uptake and subsequent intracellular distribution (e.g., endosome/lysosome, cytosol, and nucleus) of exogenous DNA transfected by viral and nonviral vectors in living cells, using a combination of TaqMan PCR and a recently developed confocal image-assisted three-dimensionally integrated quantification method. As a model, adenovirus (Ad) and Lipofectamine Plus (LFN) were used for comparison since they are highly potent and widely used viral and nonviral vectors, respectively. The findings indicate that the efficiency of cellular uptake for LFN is significantly higher than that for Ad. Once taken up by a cell, Ad exhibited comparable endosomal escape and slightly higher nuclear transfer efficiency compared with LFN. In contrast, LFN requires 3 orders of magnitude more intranuclear gene copies to exhibit a transgene expression comparable to that of the Ad, suggesting that the difference in transfection efficiency principally arises from differences in nuclear transcription efficiency and not from a difference in intracellular trafficking between Ad and LFN.

Key Words: adenovirus, nonviral vector, lipoplex, quantification, intracellular trafficking, gene vector

INTRODUCTION

Numerous nonviral vectors have been developed for use in gene therapy for intractable diseases [1,2]. However, low transfection efficiency still remains a bottleneck, preventing its use in clinical applications. It is generally considered that transfection activity is rate limited to a great extent, by a variety of intracellular processes such as endosomal escape, nuclear transfer, and intranuclear transcription.

Along with evolution of life during the past hundreds of millions of years, DNA and RNA viruses have also evolved and have developed sophisticated mechanisms for controlling intracellular trafficking for the efficient delivery of their genomes to nuclei in host cells for symbiosis. Although some nonviral vectors have been evolutionally developed since the first proposal of the concept of gene therapy over 30 years ago [3], this history is overwhelmingly short. Therefore, the transfection efficiency of a virus vector is, in general, more prominent than that of a nonviral vector [4]. To improve nonviral vectors, quantitative information concerning why and to what extent the nonviral vector is inferior to the viral one is essential.

For the quantification of intracellular trafficking, we and other researchers have developed methodology to quantify the amount of plasmid DNA in the nucleus by nuclear fractionation followed by the polymerase chain reaction (PCR) [5–7]. This quantification revealed an important lesson showing that it is necessary to optimize not only the nuclear delivery of plasmid DNA, but also intranuclear transcription efficiency, since transgene expression is remarkably saturated against nucleus-delivered pDNA. In contrast to the nucleus, very few reports are available concerning the amount of pDNA in the

1525-0016/$30.00

doi:10.1016/j.ymthe.2005.10.007

endosome/lysosome compartment, and therefore, it is very difficult to evaluate the efficiency of endosomal release. Although the subcellular fractionation of endosomes/lysosomes may solve this issue, many problems, such as the complicated protocol, uncertainties associated with the recovery of the endosomal fraction, and mutual contamination may prevent this strategy from becoming a practical application.

We recently developed a novel strategy, the confocal image-assisted three-dimensionally integrated quantification (CIDIQ) method, which enables the distribution of exogenous DNA in endosome/lysosome, cytosol, and nucleus to be quantified simultaneously in individual cells with sequential *Z*-series images captured by confocal laser scanning microscopy [8,9]. Since intracellular trafficking investigated by CIDIQ can readily explain the differences in transgene expression by various nonviral vectors, this method is useful for identifying the rate-limiting barriers to gene expression.

In the present study, we applied it to the systematic and quantitative comparison of the intracellular distribution of exogenous genes transfected by viral vector and nonviral vector in living cells. It enabled us to examine the rate-limiting processes associated with nonviral vectors that limit their transfection efficiency. As model vectors, we used adenovirus (Ad) and Lipofectamine Plus (LFN), highly potent and widely used viral and nonviral vectors (lipoplex), respectively, in the comparative study.

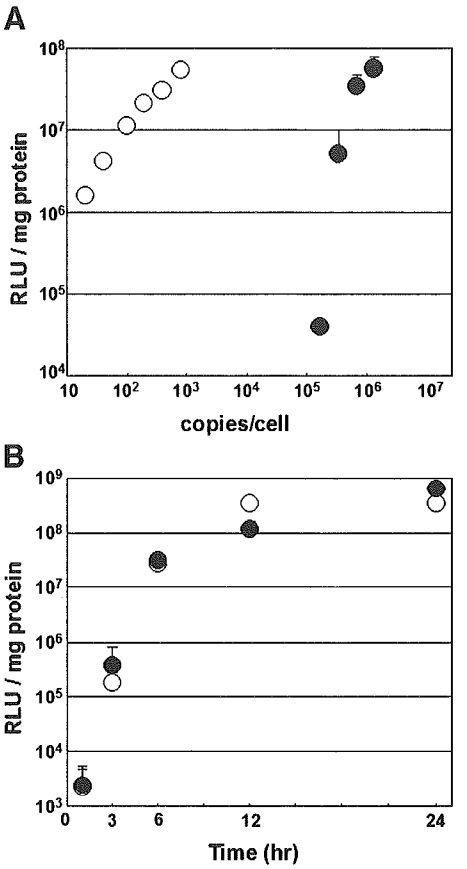

FIG. 1. Dose–response curve and time course of luciferase gene expression in A549 cells transfected by Ad and LFN. (A) Luciferase gene expression in cells transfected by Ad (○) or LFN (●) was measured 6 h after incubation at the indicated dose. (B) Transfection activities were measured at indicated times after incubation with a dose of 200 (○) or 6.7 × 10^5 copies/cell (5 pg/cell) (●). The vertical axis represents luciferase activity expressed as relative light units (RLU)/mg protein. These data represent the mean values and standard deviation of three experiments.

RESULTS

Comparison of Transfection Activity between Ad and LFN

We initially compared the time-dependent and applied dose-dependent transfection activity between Ad and LFN. The methodology used to determine the applied dose in terms of luciferase gene copies is described under Materials and Methods. As shown in Fig. 1A, transgene expression is increased in a dose-dependent manner for both vectors 6 h after incubation. In subsequent experiments, we fixed the dose of plasmid DNA (pDNA) in the LFN-mediated transfection at 6.7 × 10^5 copies/cell (5 pg/cell) based on the manufacturer's recommended protocol, from which approximately 5 × 10^7 RLU/mg protein of luciferase activity was exhibited. In the case of Ad, we fixed the dose at 200 copies/cell, since comparable levels of transgene expression can be achieved at this dose. As shown in Fig. 1B, both vectors exhibited quite comparable time courses for transgene expression at these doses, suggesting that LFN is a potent system for the delivery of pDNA to the nucleus with a speed comparable to that of Ad. However, it should be emphasized that LFN requires 3 orders of magnitude more gene copies than the Ad to achieve comparable gene expression (Fig. 1A). Furthermore, the difference in the required dose for achieving a comparable level of transgene expression is dependent on the expression level. In a comparison of the expression of 1 × 10^6 RLU/mg protein, approximately 10,000-fold more copies of plasmid DNA were required for LFN, and at a lower transgene expression level, the difference was even greater. This is due to the nonlinear relationship between the dose and the transfection efficiency in LFN and is also sometimes observed in various nonviral vectors [10].

Quantification of an Intracellular Distribution of pDNA and Ad DNA

We then quantified the intracellular distribution of pDNA or Ad by a combination of TaqMan PCR and CIDIQ [8]. The procedures used to determine the distribution of exogenous DNA transfected by LFN and Ad are

doi:10.1016/j.ymthe.2005.10.007

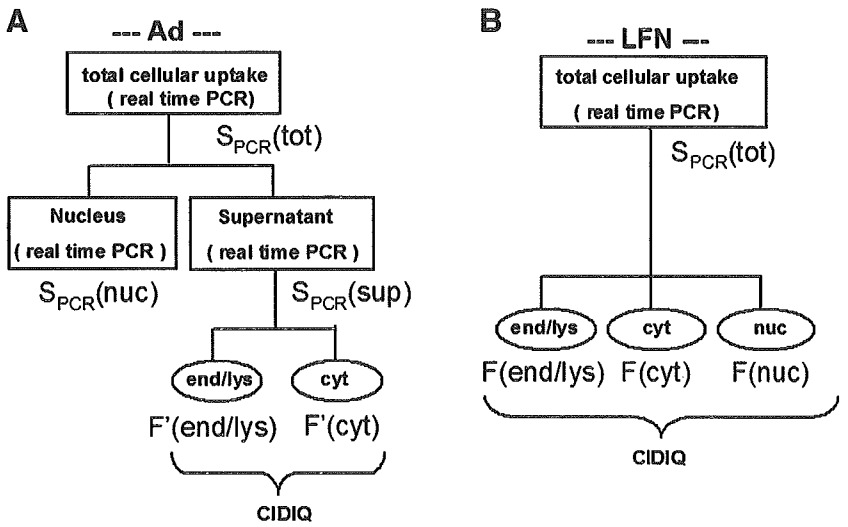

FIG. 2. Schematic diagram illustrating the concept for the quantification of intracellular distribution of exogenous genes. Subcellular distributions of exogenous DNA transfected by Ad and LFN were quantified by TaqMan PCR and CIDIQ analysis as illustrated in (A) and (B), respectively. (A) Total cellular uptake (S_{PCR}(tot) and nuclear-delivered Ad DNA (S_{PCR}(nuc)) were quantified by TaqMan PCR. Distributions of Ad in endosome/lysosome and cytosol (F'(end/lys) and F'(cyt), respectively) were also determined by CIDIQ. The copy numbers in the endosome/lysosome and cytosol fractions were calculated as S_{PCR}(sup) multiplied by F'(end/lys) and F'(cyt), respectively. (B) S_{PCR}(tot) was first determined by TaqMan PCR in terms of gene copies. The fraction of plasmid DNA in the endosome/lysosome, cytosol, and nucleus was determined by CIDIQ.

illustrated in Figs. 2A and 2B. We determined the total cellular uptake (S_{PCR}(tot)) first by TaqMan PCR in terms of gene copies. In the case of LFN, we determined the fraction of plasmid DNA in the endosome/lysosome, cytosol, and nucleus by CIDIQ (Fig. 2B). A schematic diagram illustrating the principal of CIDIQ analysis is shown in Fig. 4A. After the transfection of rhodamine-labeled pDNA, we stained the endosome/lysosome and nucleus with LysoSensor DND-189 and Hoechst 33342, respectively, to discriminate the subcellular localization of the pDNA (typical images are exhibited in Fig. 4C). We transferred each 8-bit TIFF image to Image-Pro Plus version 4.0 (Media Cybernetics, Inc., Silver Spring, MD, USA) to quantify the total brightness and pixel area of each region of interest. Since we have previously shown that the majority of rhodamine-labeled pDNA was present in the form of clusters in the cytosol and nucleus at 1 h (a typical image is shown in Fig. 4C), we used the pixel area of each cluster in endosomes/lysosomes, s_i(end/lys); cytosol, s_i(cyt); and nucleus, s_i(nuc) as an index of the amount of pDNA [8]. The detailed methodology for the calculation of the fraction of pDNA in the endosome/lysosome, cytosol, and nucleus (F(end/lys), F(cyt), and F(nuc), respectively) is described under Materials and Methods. The copy number in each organelle is calculated as S_{PCR}(tot) multiplied by the fraction in each organelle (Fig. 2B).

We also determined intracellular distribution for the Ad by CIDIQ (a typical image is shown in Fig. 4B), in which the pixel areas of the Texas red-labeled Ad are used as an index of the amount of Ad. However, the nuclear pixels cannot serve as an index for the amount of Ad DNA, since it is dissociated from the fluorescence-labeled capsid proteins when it is internalized via the nuclear pore complex [11]. Therefore, we determined nucleus-associated Ad DNA (S_{PCR}(nuc)) beforehand by nuclear isolation, followed by TaqMan PCR (Fig. 2A). In this case, the supernatant from the nuclear isolation procedure (S_{PCR}(sup)) includes DNA in both the endosomal/lysosome and the cytosol fractions. The copy numbers in these fractions are calculated as S_{PCR}(sup) multiplied by the fractions calculated by CIDIQ (F'(end/lys) and F'(cyt), respectively).

Comparison of the Cellular Uptake Process between LFN and Ad

We first quantified the cellular uptake of pDNA transfected with LFN and Ad in terms of copy numbers of luciferase genes by TaqMan PCR. Since the nuclear delivery of exogenous DNA is achieved within 1 h for both of vectors [8,12–14], we evaluated cellular uptake and the following intracellular distribution at 1 h to compare the initial disposition of DNA. As a result, the number of copies of pDNA taken up by the cell for LFN was approximately 15,000-fold more than that for Ad (Fig. 3). After we normalized the cellular uptake by the applied dose, more

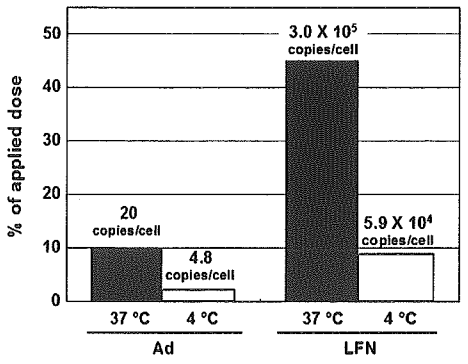

FIG. 3. Quantification of cellular uptake and cellular binding of Ad and LFN in A549 cells. A549 cells were incubated with adenovirus or LFN at 37 and 4°C for 1 h to evaluate cellular uptake and cellular binding, respectively. Associated genes were quantified in terms of copy number of luciferase genes by TaqMan PCR. Cellular association was normalized by number of cells, which was quantified by the number of copies of the genomic β-actin gene.

doi:10.1016/j.ymthe.2005.10.007

than 40% of the pDNA was taken up by the cell, whereas for the Ad DNA, this value was only 10% (Fig. 3).

Total cellular uptake is a hybrid parameter of cell surface binding and the internalization rate constant (k_{int}). Therefore, we measured the cellular binding of pDNA and Ad by incubation at 4°C for 1 h. In the case of LFN, 8.8% of the applied pDNA was attached to the cell surface, whereas the corresponding value was only 2.4% for the Ad (Fig. 3). When the k_{int}, denoted as the total cellular uptake (Fig. 3) divided by the cell surface binding (Fig. 3), were compared, LFN was found to exhibit a value comparable to that of Ad (5.1 and 4.2 h^{-1}, respectively).

Comparison of Intracellular Trafficking between Ad and LFN

Concerning the intracellular distribution after transfection with LFN, 47.4% of the pDNA was in the endosome/lysosome fraction and a large part of the pDNA had already escaped from this compartment (Figs. 4E and 5) within 1 h. In addition, we observed significant nuclear distribution (13.5%) (Figs. 4E and 5). This is consistent with rapid gene expression within 3 h (Fig. 1B). Multiplying these fractions by the S_{PCR}(tot), we calculated the copy numbers in each organelle as shown in Fig. 5.

In the Ad, we determined nuclear fraction by nuclear isolation, followed by TaqMan PCR. After incubation at 37°C at 1 h, 54.2% of the Ad genome was experimentally recovered from the nuclear fraction. To avoid a situation in which the nuclear delivery of the Ad genome was overestimated, we estimated the efficiency of contamination of Ad in the nucleus during the nuclear isolation with cells that were incubated with Ad at 4°C, at which temperature nuclear delivery was largely excluded. After incubation at 4°C for 1 h, we fractionated the nucleus and quantified cell surface-bound and nucleus-associated Ad. As a result, we calculated the percentage of nuclear Ad to cell surface-bound Ad to be 17.6%. Thus, 17.6% of the nuclear fraction, corresponding to contamination during the isolation process, was subtracted from the experimentally determined nuclear fraction after the incubation at 37°C (54.2%). As a result, we calculated that 36.6% of the total cellular uptake (7.3 copies/nucleus) of DNA reached the nucleus (Fig. 5). Other portions (12.7 copies/cell; 63.4% of the total cellular uptake) were recovered from the supernatant fractions (S_{PCR}(sup)), which include the endosome/lysosome and cytosol fractions. A CIDIQ analysis showed that the fractions in the endosome/lysosome (F'(end/lys)) and the cytosol (F'(cyt)) compared to the supernatant were 47.9 and 52.1%, respectively. Taking these data into consideration, we calculated the numbers of Ad gene copies in the endosome/lysosome and cytosol as 6.1 copies/cell (30.3% of the total cellular uptake) and 6.6 copies/cell (33.1% of the total cellular uptake), respectively (Figs. 4D and 5). The efficiency of the endosomal escape and nuclear translocation calculated from the data shown in the circle graph in Fig. 5 is summarized in Table 1. We calculated the efficiency of endosomal escape as the fraction that escaped from the endosome/lysosome (nuclear fraction plus cytoplasmic fraction) divided by the total cellular uptake. Similarly, we determined the efficiency of nuclear translocation as the nuclear fraction divided by the fraction that escaped from the endosome/lysosome (nuclear fraction plus cytoplasmic fraction). As a result, the efficiency of endosomal escape is only slightly higher for Ad. In contrast, the efficiency of nuclear translocation is considerably higher for Ad.

Finally, comparing the nuclear delivery of DNA, 5600-fold more gene copies are delivered to the nucleus in the case of LFN. We calculated transcription efficiency as the expression divided by the gene copies in the nucleus as shown in Fig. 5. It was shown that Ad is 8100 times more efficient than LFN in nuclear transcription.

This conclusion is also applicable to HeLa cells (Table 2). To exhibit a comparable transgene expression, LFN also requires 3 orders of magnitude more gene copies (200 vs 1.4×10^6 copies/cell). Under these conditions, approximately 4100 times more gene copies reach the nucleus, and therefore, the transcription efficiency of Ad was approximately 7000 times higher than that of LFN.

Discussion

In the present study, intracellular trafficking and the intranuclear transcription of exogenous DNA transfected by viral and nonviral vectors were quantitatively evaluated. Ad and LFN were used as model vectors in the comparison, since they are both highly potent and widely used vectors. As a result, we found that LFN can accomplish transgene expression comparable to that of the Ad vector, when the protocol is optimized. However, the dose of pDNA in terms of luciferase gene copies under these conditions was 3 orders of magnitude more than that of Ad. Therefore, it would be worthwhile to clarify which of the intracellular processes is rate limiting for LFN.

First, the cellular uptake process was compared. Calculated from the applied dose and cellular uptake (Fig. 3), LFN exhibited significantly higher cellular uptake efficiency than Ad (approximately 45% vs 10%). Further comparison of the cellular binding efficiency by incubation at 4°C (Fig. 3) indicated that the efficient cellular uptake in the case of LFN can be attributed to efficient cellular binding, but not to the internalization rate constant (k_{int}). The superior cellular surface binding in the case of LFN can be explained by differences in the binding mechanism. Binding of the Ad is based on specific ligand–receptor interactions between the fiber protein and the coxsackievirus and Ad receptor and between the RGD motif in the penton base and the integrin receptors [15]. Therefore, the maximum binding is dependent on the total number of these receptors. In

doi:10.1016/j.ymthe.2005.10.007

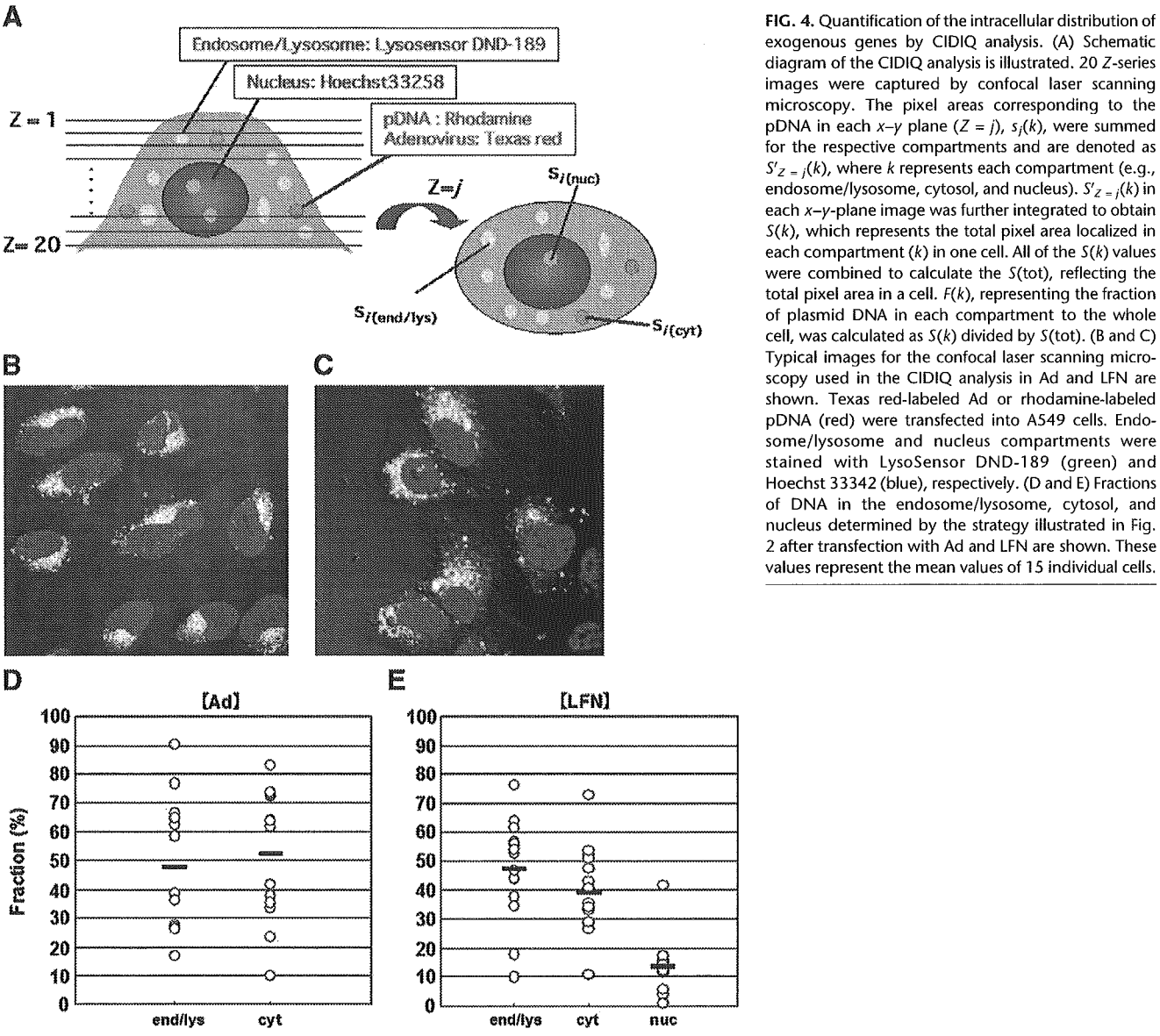

FIG. 4. Quantification of the intracellular distribution of exogenous genes by CIDIQ analysis. (A) Schematic diagram of the CIDIQ analysis is illustrated. 20 *Z*-series images were captured by confocal laser scanning microscopy. The pixel areas corresponding to the pDNA in each *x*–*y* plane ($Z = j$), $s_j(k)$, were summed for the respective compartments and are denoted as $S'_{Z=j}(k)$, where *k* represents each compartment (e.g., endosome/lysosome, cytosol, and nucleus). $S'_{Z=j}(k)$ in each *x*–*y*-plane image was further integrated to obtain $S(k)$, which represents the total pixel area localized in each compartment (k) in one cell. All of the $S(k)$ values were combined to calculate the S(tot), reflecting the total pixel area in a cell. $F(k)$, representing the fraction of plasmid DNA in each compartment to the whole cell, was calculated as $S(k)$ divided by S(tot). (B and C) Typical images for the confocal laser scanning microscopy used in the CIDIQ analysis in Ad and LFN are shown. Texas red-labeled Ad or rhodamine-labeled pDNA (red) were transfected into A549 cells. Endosome/lysosome and nucleus compartments were stained with LysoSensor DND-189 (green) and Hoechst 33342 (blue), respectively. (D and E) Fractions of DNA in the endosome/lysosome, cytosol, and nucleus determined by the strategy illustrated in Fig. 2 after transfection with Ad and LFN are shown. These values represent the mean values of 15 individual cells.

contrast, the pDNA/LFN complex can bind to the entire cell surface area via electrostatic interactions. Concerning the k_{int} value, it has recently been reported that Ad enters, not only via clathrin-mediated endocytosis [16,17], but also via macropinocytosis [18,19], which is actively driven by signal transduction after the binding of the RGD motif to the integrin receptor for cellular entry [20–22]. Therefore, the internalization of Ad appears to be a highly efficient process. The k_{int} value of LFN was comparable to that of Ad. A recent study indicated that a certain type of nonviral vector was taken up by cells, not only by the classical endocytosis pathway [23,24], but also by another pathway such as macropinocytosis [25]. Presumably, multiple pathways are also responsible to the cellular uptake of LFN, and this results in an internalization rate constant comparable to that of Ad. Concerning intracellular trafficking, various types of cellular uptake processes must be considered. Since only acidic compartments were stained by LysoSensor DND-189, the involvement of nonacidic vesicular compartments such as caveola was excluded from the analysis. To analyze the contribution of acidic vesicular transport (i.e., clathrin-mediated endocytosis and macropinocytosis [26]) to total vesicular transport, plasma membranes were nonspecifically labeled with PKH-26 (Sigma). After incubation for 1 h, all of the labels on the plasma membrane were internalized and detected as clustered forms. Dual staining with PKH-26 and LysoSensor DND-189 revealed that approximately 70% of the PKH-26 clusters were colocalized with LysoSensor DND-189, suggesting that a major

doi:10.1016/j.ymthe.2005.10.007

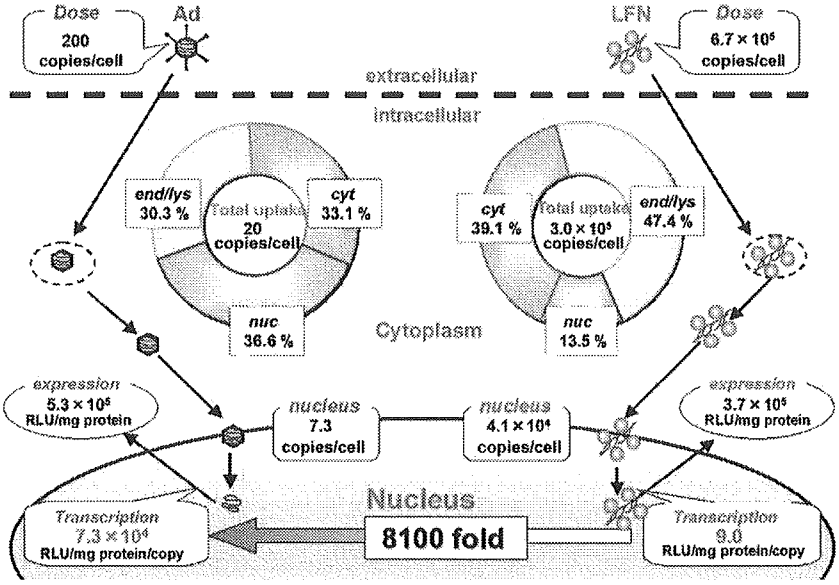

FIG. 5. Summary of the quantitative comparison of intracellular trafficking in A549 cells between Ad and LFN. These values were quantified by TaqMan PCR and CIDIQ analysis.

part (~70%) of the vesicular transport system was acidic compartments (data not shown). In addition, it appears that the size of the lipoplex (generally more than 200 nm [27,28]) is too large to be taken up via nonacidic vesicular transport such as caveolin-mediated endocytosis (~60 nm) and clathrin- and caveolin-independent endocytosis (~90 nm) [29]. Therefore, we conclude that the staining of vesicular compartments by LysoSensor DND-189 is useful for tracing the main intracellular trafficking of vectors, although it is possible that pDNA taken up via a nonacidic compartment may unexpectedly participate in the efficient trafficking pathway. The mechanism for the efficient internalization rate of the LFN remains to be clarified.

Concerning endosomal escape, it was considered that the dismantling of Ad particles in response to the low endosomal pH is closely related to this event [16,30]. Wiethoff *et al.* have recently shown that partial disassembly of the Ad capsid triggers the release of protein VI, which then lyses the endosomal membrane structure [31]. LFN also had an efficiency comparable to that of adenovirus (Table 1). LFN consists of polycationic lipid 2,3-dioleyloxy-*N*-[2(spermincarboxamido)ethyl]-*N*,*N*-dimethyl-1-propanaminium trifluoroacetate (DOSPA) and corn-shape lipid dioleoyl phosphatidylethanolamine (DOPE). A highly efficient endosomal escape of LFN, as high as that of Ad, was then synergistically achieved by the proton sponge effect [32] derived from secondary amines in DOSPA, along with the fusogenic effect [33,34] of DOPE, whereas their strategies were different.

In contrast, once it escapes into the cytosol, adenovirus delivers its DNA to the nucleus more efficiently than LFN. Although LFN can rapidly deliver its DNA to the nucleus presumably due to the electric interaction of cationic lipid and negatively charged lipids of the nuclear membrane [35], it is likely that the cytoplasmic delivery of Ad is more sophisticated. It has previously been shown that Ad utilizes a microtubule network to pass through the cytoplasm into the nucleus [36,37]. Furthermore, Ad binds to the nuclear pore complex receptor CAN/Nup214 and, thereafter, inserts the genomic DNA into the nucleus with the assistance of

TABLE 1: Comparison of the efficiencies of endosomal escape and nuclear translocation between Ad and LFN

	Ad	LFN
Endosomal escape; (cytosol + nucleus)/total	0.70	0.53
Nuclear translocation; nucleus/(nucleus + cytosol)	0.53	0.26

The efficiencies of endosomal escape and nuclear translocation were calculated from the results in Fig. 5 (circle graph) as the fraction that escaped from the endosome/lysosome (nuclear fraction plus cytoplasmic fraction) divided by total cellular uptake and as the nuclear fraction divided by the fraction that escaped from the endosome/lysosome, respectively.

TABLE 2: Comparison of nuclear delivery and transcription efficiency between Ad and LFN in HeLa cells

	Ad	LFN
Dose (copies/cell)	200	1.4×10^6
Nuclear DNA (copies/cell)	4.1	1.7×10^4
Transgene expression (RLU/mg protein)	2.3×10^7	1.3×10^7
Transcription efficiency (RUL/mg protein/copy)	5.7×10^6	810

The numbers of gene copies required to exhibit comparable transgene expression were quantified by TaqMan PCR and are represented as copies/cell. Nuclear DNA in Ad- and LFN-mediated transfection was determined following the procedure illustrated in Fig. 2. Transcription efficiency was calculated as the expression divided by the gene copies in the nucleus.

doi:10.1016/j.ymthe.2005.10.007

nuclear histone H1 cells and the importin family proteins of the host cells [11,38]. Such types of multiple/active delivery systems in adenovirus may be responsible for its efficient nuclear delivery.

Finally, the intranuclear transcription of DNA, when transfected with Ad, is 8100 times higher than that of LFN. Considering that the CMV promoter, luciferase (GL3), and BGH polyadenylation sequences in pDNA and the Ad genome are identical to one another, two explanations are possible. One is that the nuclear DNA introduced by the LFN is so well condensed that the transcription process is inhibited. It is generally accepted that the release of pDNA from the vectors is the rate-determining process for transgene expression [39]. In fact, transgene expression after the nuclear microinjection of DNA as a lipoplex was reported to be severely limited [28,40]. The other possibility is that the Ad genome structure and/or proteins coded in the Ad genome affect transgene expression. Since almost all of the E1/E3 region was deleted from the Ad genome, other factors such as the inverted terminal repeat sequence [41], terminal protein [42], and various proteins derived from the E4 region [43,44] may be involved in the improvement in transcription and nuclear stability. Currently, it has been reported that terminal proteins interact with the nuclear matrix, where they play an important role in nuclear transcription [42]. To evaluate the potential of pDNA vis-a-vis adenovirus DNA in the transcription process, adenoviral DNA was purified by treatment with guanidine, followed by sucrose gradient centrifugation [45]. The nuclear microinjection of 10 copies of plasmid DNA and Ad genome encoding the green fluorescent protein revealed that the Ad genome exhibited only a slightly higher transgene expression compared with plasmid DNA (approximately 35% vs 25%), suggesting that these two types of DNA are equivalent in the transcription process (S. Hama *et al.*, unpublished observation). As a result, the difference in decondensation in the nucleus is a more plausible hypothesis for explaining the difference in intranuclear transcription.

The remarkable difference in transcription activity was also found in HeLa cells, indicating that this phenomenon is generally applicable to various cells. Very recently, it was also shown that the intranuclear transcription of plasmid DNA introduced by nonviral vectors such as polyethylenimine was much lower than that of viral vectors. This conclusion is then generally applicable to various types of current nonviral vectors [46].

Collectively, we were able successfully to quantify the intracellular trafficking and intranuclear transcription of viral and nonviral vectors. LFN delivers pDNA to the nucleus with a comparable speed and exhibits transgene expression comparable to that of the Ad vector. However, LFN requires 3 orders of magnitude more pDNA than the Ad to exert similar transfection activities. Surprisingly, this remarkable difference principally arises from differences in nuclear transcription efficiency. This is the first systematic and quantitative comparison of the intracellular distribution of the exogenous genes introduced by a viral vector and a nonviral vector. Such quantitative comparisons will be useful for developing new generations of nonviral vectors.

Materials and Methods

General. To prepare the reporter gene vector for the pDNA (pcDNA3.1-GL3), an insert fragment encoding luciferase (GL3) was obtained by *Hin*dIII/*Xba*I digestion of the pGL3-Basic vector (Promega, Madison, WI, USA) and ligated to the *Hin*dIII/*Xba*I-digested site of pcDNA3.1 (Invitrogen, Carlsbad, CA, USA). LFN was from Invitrogen Corp. Other chemicals used were commercially available and reagent grade products. As to the viral vector, the $E1^-$, $E3^-$, replication-deficient serotype 5 adenovirus, in which an expression cassette is inserted in the E_1 position, was used [47]. The expression cassette consists of a cytomegalovirus promoter/enhancer, cDNA encoding luciferase (GL3), and BGH polyadenylation sequences, which are also encoded in the pDNA used in the LFN-mediated transfection.

Quantification of luciferase gene copies by TaqMan PCR. To determine the applied particle titer of the Ad in terms of copy number of luciferase gene, Ad was dismantled by vortexing with 0.1% SDS/10 mM Tris–HCl/5 mM EDTA treatment. The number of luciferase gene copies was determined by TaqMan PCR with a 100-fold diluted sample solution. As a reference, a dilution series of pDNA3.1-GL3 was run along with the virus sample. It was confirmed that 0.001% SDS and 0.05 mM EDTA had no effect on the luciferase gene amplification by TaqMan PCR. The luciferase gene region of Ad genomic DNA or pDNA was amplified and quantified by TaqMan PCR (ABI Prism 7700 sequence detection system; Applied Biosystems). The sequence of the probe was 5′-CCGCTGAATTG-GAATCCATCTTGCTC-3′ with FAM as a fluorescent dye on the 5′ end and TAMRA as a fluorescence quencher dye labeled on the 3′ end. This probe is designed to anneal to the target between the sense primer (5′-TTGACCGCCTGAAGTCTCTGA-3′) and the antisense primer (5′-ACACCTGCGTCGAAGATGTTG-3′) in the luciferase sequence of the Ad genome and pDNA.

For the quantification of cellular uptake and nuclear delivery of the luciferase genes, DNA was purified from cell lysates or an isolated nucleus by means of a GenElute Mammalian Genome DNA Miniprep kit (Sigma–Aldrich, St. Louis, MO, USA) and subjected to the TaqMan PCR with ABI Prism 7700 sequence detection system. The isolation of nuclei followed a previous report [6,7]. Briefly, cells were suspended in 0.5 ml of lysis buffer (0.5% Nonidet P-40, 10 mM NaCl, 3 mM $MgCl_2$, 10 mM Tris–HCl buffer; pH 7.4) to dissolve the plasma membrane, and the nuclear fraction was then isolated by centrifugation at 1400*g* for 5 min. This treatment (washing) was repeated twice, and the final pellet was used as the nuclear fraction. The high recovery of the Ad genome (>90%) by DNA purification with the GenElute Mammalian Genome DNA Miniprep kit was confirmed by comparison with the luciferase gene amplification by TaqMan PCR.

The number of β-actin DNAs was also determined by the ABI Prism 7700 sequence detection system. PCR was performed according to the manufacturer's instructions with 0.5 μM each forward, 5′-TGCGTGACAT-TAAGGAGAAGCTGTG-3′, and reverse, 5′-CAGCGGAACCGCTCATTGC-CAATGG-3′, primers and the QuantiTect SYBR Green PCR Master Mix (Qiagen, Hilden, Germany). A linear relationship between the number of cells and the threshold cycle for the β-actin gene amplification was confirmed (data not shown).

CIDIQ analysis. In the case of LFN-mediated transfection, the pDNA fraction in the endosome/lysosome, cytosol, and nucleus compared to the total cellular association was assessed by CIDIQ, as described in a recent report [8]. After the transfection of rhodamine-labeled pDNA, the endo-

doi:10.1016/j.ymthe.2005.10.007

some/lysosome and nucleus were stained with LysoSensor DND-189 and Hoechst 33342, respectively, to discriminate the subcellular localization of pDNA. Each 8-bit TIFF image was transferred to Image-Pro Plus version 4.0 (Media Cybernetics, Inc.) to quantify the total brightness and pixel area of each region of interest. For data analysis, the pixel areas of each cluster in endosomes/lysosomes, s_i(end/lys); cytosol, s_i(cyt); and nucleus, s_i(nuc) were separately summed for each x–y plane and are denoted as $S'_{Z=i}$(end/lys), $S'_{Z=i}$(cyt), and $S'_{Z=i}$(nuc), respectively. The values of $S'_{Z=i}$(end/lys), $S'_{Z=i}$(cyt), and $S'_{Z=i}$(nuc) in each x–y plane were further summed and are denoted as S(end/lys), S(cyt), and S(nuc), respectively. These parameters represent the total amount of pDNA in each compartment in an individual cell. Furthermore, the total area of the pDNA, denoted as S(tot), was calculated by integrating the S(end/lys), S(cyt), and S(nuc). This value represents the total cellular uptake of pDNA. The fractions of pDNA present in endosomes/lysosomes, cytosol, and nucleus compared to the whole cell are denoted as F(end/lys), F(cyt), and F(nuc), which were calculated as S(end/lys), S(cyt), and S(nuc) divided by S(tot), respectively.

For quantification of the intracellular distribution of Ad, Texas red-labeled Ad was used in the CIDIQ analysis. The nuclear delivery of Ad DNA (S_{PCR}(nuc)) was quantified beforehand by nuclear fractionation, followed by the TaqMan PCR [6]. The supernatant fraction S_{PCR}(sup) contains Ad DNA in the endosome/lysosome and cytosol. Therefore, the fractions in these organelles were quantified by CIDIQ. In this case, S(sup), which represents the Ad DNA in the supernatant fraction in the nucleus isolation experiment, was calculated by integrating the S'(end/lys) and S'(cyt). The fractions of Ad DNA present in endosomes/lysosomes and cytosol compared to the supernatant are denoted as F'(end/lys) and F'(cyt), which were calculated as S'(end/lys) and S'(cyt) divided by S(sup), respectively. Numbers of gene copies in these organelles were determined by multiplying each fraction by S_{PCR}(sup).

ACKNOWLEDGMENTS

This work was supported in part by Grants-in-Aid for Scientific Research (B) and Grant-in-Aid for Young Scientists (B) from the Ministry of Education, Culture, Sports, Science, and Technology of Japan and by Grants-in-Aid for Scientific Research on Priority Areas from the Japan Society for the Promotion of Science.

RECEIVED FOR PUBLICATION JUNE 11, 2005; REVISED SEPTEMBER 30 2005; ACCEPTED OCTOBER 1, 2005.

REFERENCES

1. Lai, C. M., Lai, Y. K., and Rakoczy, P. E. (2002). Adenovirus and adeno-associated virus vectors. *DNA Cell Biol.* **21:** 895–913.
2. Yoshida, J., *et al.* (2004). Human gene therapy for malignant gliomas (glioblastoma multiforme and anaplastic astrocytoma) by in vivo transduction with human interferon beta gene using cationic liposomes. *Hum. Gene Ther.* **15:** 77–86.
3. Friedmann, T., and Roblin, R. (1972). Gene therapy for human genetic disease? *Science* **175:** 949–955.
4. Dinser, R., *et al.* (2001). Comparison of long-term transgene expression after non-viral and adenoviral gene transfer into primary articular chondrocytes. *Histochem. Cell Biol.* **116:** 69–77.
5. Oh, Y. K., *et al.* (2002). Polyethylenimine-mediated cellular uptake, nucleus trafficking and expression of cytokine plasmid DNA. *Gene Ther.* **9:** 1627–1632.
6. Tachibana, R., *et al.* (2002). Quantitative analysis of correlation between number of nuclear plasmids and gene expression activity after transfection with cationic liposomes. *Pharm. Res.* **19:** 377–381.
7. Tachibana, R., Harashima, H., Shinohara, Y., and Kiwada, H. (2001). Quantitative studies on the nuclear transport of plasmid DNA and gene expression employing nonviral vectors. *Adv. Drug Delivery Rev.* **52:** 219–226.
8. Akita, H., Ito, R., Khalil, I. A., Futaki, S., and Harashima, H. (2004). Quantitative three-dimensional analysis of the intracellular trafficking of plasmid DNA transfected by a nonviral gene delivery system using confocal laser scanning microscopy. *Mol. Ther.* **9:** 443–451.
9. Masuda, T., Akita, H., and Harashima, H. (2005). Evaluation of nuclear transfer and transcription of plasmid DNA condensed with protamine by microinjection: the use of a nuclear transfer score. *FEBS Lett.* **579:** 2143–2148.
10. Moriguchi, R., *et al.* (in press). Non-linear pharmacodynamics in a non-viral gene delivery system: positive non-linear relationship between dose and transfection efficiency. *J. Controlled Release.*
11. Trotman, L. C., Mosberger, N., Fornerod, M., Stidwill, R. P., and Greber, U. F. (2001). Import of adenovirus DNA involves the nuclear pore complex receptor CAN/Nup214 and histone H1. *Nat. Cell Biol.* **3:** 1092–1100.
12. Leopold, P. L., *et al.* (1998). Fluorescent virions: dynamic tracking of the pathway of adenoviral gene transfer vectors in living cells. *Hum. Gene Ther.* **9:** 367–378.
13. Miyazawa, N., *et al.* (1999). Fiber swap between adenovirus subgroups B and C alters intracellular trafficking of adenovirus gene transfer vectors. *J. Virol.* **73:** 6056–6065.
14. Nakano, M. Y., and Greber, U. F. (2000). Quantitative microscopy of fluorescent adenovirus entry. *J. Struct. Biol.* **129:** 57–68.
15. Meier, O., and Greber, U. F. (2003). Adenovirus endocytosis. *J. Gene Med* **5:** 451–462.
16. Greber, U. F., Willetts, M., Webster, P., and Helenius, A. (1993). Stepwise dismantling of adenovirus 2 during entry into cells. *Cell* **75:** 477–486.
17. Varga, M. J., Weibull, C., and Everitt, E. (1991). Infectious entry pathway of adenovirus type 2. *J. Virol.* **65:** 6061–6070.
18. Imelli, N., Meier, O., Boucke, K., Hemmi, S., and Greber, U. F. (2004). Cholesterol is required for endocytosis and endosomal escape of adenovirus type 2. *J. Virol.* **78:** 3089–3098.
19. Meier, O., *et al.* (2002). Adenovirus triggers macropinocytosis and endosomal leakage together with its clathrin-mediated uptake. *J. Cell Biol.* **158:** 1119–1131.
20. Amyere, M., *et al.* (2000). Constitutive macropinocytosis in oncogene-transformed fibroblasts depends on sequential permanent activation of phosphoinositide 3-kinase and phospholipase C. *Mol. Biol. Cell.* **11:** 3453–3467.
21. Araki, N., Johnson, M. T., and Swanson, J. A. (1996). A role for phosphoinositide 3-kinase in the completion of macropinocytosis and phagocytosis by macrophages. *J. Cell Biol.* **135:** 1249–1260.
22. Li, E., Stupack, D., Klemke, R., Cheresh, D. A., and Nemerow, G. R. (1998). Adenovirus endocytosis via alpha(v) integrins requires phosphoinositide-3-OH kinase. *J. Virol.* **72:** 2055–2061.
23. Zhou, X., and Huang, L. (1994). DNA transfection mediated by cationic liposomes containing lipopolylysine: characterization and mechanism of action. *Biochim. Biophys. Acta* **1189:** 195–203.
24. Zuhorn, I. S., Kalicharan, R., and Hoekstra, D. (2002). Lipoplex-mediated transfection of mammalian cells occurs through the cholesterol-dependent clathrin-mediated pathway of endocytosis. *J. Biol. Chem.* **277:** 18021–18028.
25. Goncalves, C., *et al.* (2004). Macropinocytosis of polyplexes and recycling of plasmid via the clathrin-dependent pathway impair the transfection efficiency of human hepatocarcinoma cells. *Mol. Ther.* **10:** 373–385.
26. Wadia, J. S., Stan, R. V., and Dowdy, S. F. (2004). Transducible TAT-HA fusogenic peptide enhances escape of TAT-fusion proteins after lipid raft macropinocytosis. *Nat. Med.* **10:** 310–315.
27. Joshee, N., Bastola, D. R., and Cheng, P. W. (2002). Transferrin-facilitated lipofection gene delivery strategy: characterization of the transfection complexes and intracellular trafficking. *Hum. Gene Ther.* **13:** 1991–2004.
28. Zabner, J., Fasbender, A. J., Moninger, T., Poellinger, K. A., and Welsh, M. J. (1995). Cellular and molecular barriers to gene transfer by a cationic lipid. *J. Biol. Chem.* **270:** 18997–19007.
29. Conner, S. D., and Schmid, S. L. (2003). Regulated portals of entry into the cell. *Nature* **422:** 37–44.
30. Medina-Kauwe, L. K. (2003). Endocytosis of adenovirus and adenovirus capsid proteins. *Adv. Drug Delivery Rev.* **55:** 1485–1496.
31. Wiethoff, C. M., Wodrich, H., Gerace, L., and Nemerow, G. R. (2005). Adenovirus protein VI mediates membrane disruption following capsid disassembly. *J. Virol.* **79:** 1992–2000.
32. Boussif, O., *et al.* (1995). A versatile vector for gene and oligonucleotide transfer into cells in culture and in vivo: polyethylenimine. *Proc. Natl. Acad. Sci. USA* **92:** 7297–7301.
33. Bailey, A. L., and Cullis, P. R. (1997). Membrane fusion with cationic liposomes: effects of target membrane lipid composition. *Biochemistry* **36:** 1628–1634.
34. Wattiaux, R., Jadot, M., Warnier-Pirotte, M. T., and Wattiaux-De Coninck, S. (1997). Cationic lipids destabilize lysosomal membrane in vitro. *FEBS Lett.* **417:** 199–202.
35. Daum, G. (1985). Lipids of mitochondria. *Biochim. Biophys. Acta* **822:** 1–42.
36. Suomalainen, M., Nakano, M. Y., Boucke, K., Keller, S., and Greber, U. F. (2001). Adenovirus-activated PKA and p38/MAPK pathways boost microtubule-mediated nuclear targeting of virus. *EMBO J.* **20:** 1310–1319.
37. Suomalainen, M., *et al.* (1999). Microtubule-dependent plus- and minus end-directed motilities are competing processes for nuclear targeting of adenovirus. *J. Cell Biol.* **144:** 657–672.
38. Greber, U. F., *et al.* (1997). The role of the nuclear pore complex in adenovirus DNA entry. *EMBO J.* **16:** 5998–6007.
39. Bieber, T., Meissner, W., Kostin, S., Niemann, A., and Elsasser, H. P. (2002). Intracellular route and transcriptional competence of polyethylenimine–DNA complexes. *J. Controlled Release* **82:** 441–454.
40. Pollard, H., *et al.* (1998). Polyethylenimine but not cationic lipids promotes transgene delivery to the nucleus in mammalian cells. *J. Biol. Chem.* **273:** 7507–7511.
41. Hatfield, L., and Hearing, P. (1991). Redundant enhancements in the adenovirus type 5

doi:10.1016/j.ymthe.2005.10.007

inverted terminal repeat promote bidirectional transcription *in vitro* and are important for virus growth *in vivo*. *Virology* **184:** 265–276.

42. Fredman, J. N., and Engler, J. A. (1993). Adenovirus precursor to terminal protein interacts with the nuclear matrix in vivo and in vitro. *J. Virol.* **67:** 3384–3395.

43. Endter, C., and Dobner, T. (2004). Cell transformation by human adenoviruses. *Curr. Top. Microbiol. Immunol.* **273:** 163–214.

44. Tauber, B., and Dobner, T. (2001). Adenovirus early E4 genes in viral oncogenesis. *Oncogene* **20:** 7847–7854.

45. Sharp, P. A., Moore, C., and Haverty, J. L. (1976). The infectivity of adenovirus 5 DNA–protein complex. *Virology* **75:** 442–456.

46. Varga, C. M., *et al.* (2005). Quantitative comparison of polyethylenimine formulations and adenoviral vectors in terms of intracellular gene delivery processes. *Gene Ther.* **12:** 1023–1032.

47. Mizuguchi, H., *et al.* (2001). A simplified system for constructing recombinant adenoviral vectors containing heterologous peptides in the HI loop of their fiber knob. *Gene Ther.* **8:** 730–735.

HUMAN GENE THERAPY 17:264–279 (March 2006)

Modified Adenoviral Vectors Ablated for Coxsackievirus–Adenovirus Receptor, α_v Integrin, and Heparan Sulfate Binding Reduce *In Vivo* Tissue Transduction and Toxicity

NAOYA KOIZUMI,[1] KENJI KAWABATA,[1] FUMINORI SAKURAI,[1] YOSHITERU WATANABE,[2] TAKAO HAYAKAWA,[3] and HIROYUKI MIZUGUCHI[1,4]

ABSTRACT

Coxsackievirus and adenovirus receptor (CAR), α_v integrins, and heparan sulfate glycosaminoglycans (HSGs) are the tropism determinants of adenoviral (Ad) vectors *in vivo*. For the development of a targeted Ad vector, its broad tropism needs to be blocked (or reduced). We have previously developed Ad vectors with ablation of CAR, α_v integrin, and HSG binding by mutation of the FG loop in the fiber knob (deletion of T489, A490, Y491, and T492 of the fiber protein), deletion of the RGD motif of the penton base, and substitution of the fiber shaft domain for that derived from Ad type 35, respectively, and have shown that this triple-mutant Ad vector [Ad/ΔF(FG)ΔP-S35-L2] exhibits significantly lower transduction in mouse liver compared with the conventional Ad vector [Koizumi, N., Mizuguchi, H., Sakurai, F., Yamaguchi, T., Watanabe, Y., and Hayakawa, T. (2003). J. Virol. 77, 13062–13072]. In the present study, we optimized the fiber knob mutation for further reduced *in vivo* transduction and examined toxicity of the modified Ad vectors. Ad/ΔF(AB)ΔP-S35-L2, a triple-mutant Ad vector containing a mutation of the AB loop in the fiber knob (R412S, A415G, E416G, and K417G), mediated approximately 15,000- and 500-fold lower mouse liver transduction by intravenous and intraperitoneal administration, respectively, than the conventional Ad vector, and mediated 10-fold lower mouse liver transduction than did Ad/ΔF(FG)ΔP-S35-L2. Ad/ΔF(AB)ΔP-S35-L2 also exhibited lower transduction of other organs compared with Ad/ΔF(FG)ΔP-S35-L2 and the conventional Ad vector. Levels of both liver serum enzymes (aspartate transferase [AST] and alanine transferase (ALT)] and interleukin (IL)-6 in mouse serum after intravenous administration of Ad/ΔF(AB)ΔP-S35-L2 were similar to those in the nontreatment mouse serum, whereas the conventional Ad vector led to high levels of AST, ALT, and IL-6. We therefore succeeded in further improving the mutant Ad vector, abolishing both viral natural tropism and toxicity. This new Ad vector appears to be a fundamental vector for targeted gene delivery.

OVERVIEW SUMMARY

Nonspecific distribution of adenoviral (Ad) vectors in tissue after *in vivo* gene transfer is due to the relatively broad expression of coxsackievirus and adenovirus receptor (CAR) (the primary receptor), α_v integrin (the secondary receptor), and heparan sulfate (the tertiary receptor). Ad injection *in vivo* is associated with the initiation of the inflammatory response and tissue damage. In the present study, we have generated a modified Ad vector with ablation of CAR, α_v integrin, and heparan sulfate binding and examined toxicity (liver serum enzymes and interleukin-6) of the vector as well as its transduction properties. For CAR binding ablation, the AB or FG loop mutation of the fiber knob was employed, and gene transfer activity of the triple-mutant Ad vector containing the AB loop mutation was compared with that of the triple-mutant Ad vector containing the FG loop mutation and with that of the conventional Ad vector. The triple-mu-

[1]National Institute of Biomedical Innovation, Osaka 567-0085, Japan.
[2]Showa Pharmaceutical University, Tokyo 194-8543, Japan.
[3]Pharmaceuticals and Medical Devices Agency, Tokyo 100-0013, Japan.
[4]Graduate School of Pharmaceutical Sciences, Osaka University, Osaka 567-0871, Japan.

tant Ad vector containing the AB loop mutation was found to mediate significantly lower tissue transduction *in vivo*. Furthermore, this mutant Ad vector reduced (or blunted) liver toxicity and innate immunity responses (interleukin-6 production). Thus, the triple-mutant Ad vector will likely be a fundamental vector for targeted gene delivery.

INTRODUCTION

RECOMBINANT ADENOVIRAL (Ad) VECTORS are attractive vehicles for *in vitro* and *in vivo* gene transfer to a wide variety of cell types. This distribution is largely due to the relatively broad expression of the primary receptor, the coxsackievirus and adenovirus receptor (CAR), and the secondary receptor, α_v integrin, and the tertiary receptor, heparan sulfate glycosaminoglycans (HSGs). The lack of specificity limits the utility of Ad vectors in gene therapy. Targeted Ad vectors would improve not only the efficacy but also the safety profiles of the vectors by permitting the use of lower doses, which would be less toxic and potentially less immunogenic (Krasnykh *et al.*, 2000; Wickham, 2000; Mizuguchi and Hayakawa, 2004).

The initial phase of Ad infection involves at least two sequential steps. The first is attachment of the virus to the cell surface through binding of the knob domain of the fiber to CAR (Bergelson *et al.*, 1997; Tomko *et al.*, 1997). After attachment, interaction between the RGD motif of the penton bases with secondary host cell receptors, α_v integrins, facilitates internalization via receptor-mediated endocytosis (Wickham *et al.*, 1993, 1994). Furthermore, interaction between the KKTK (Lys-Lys-Thr-Lys) motif on the fiber shaft of Ad type 5 with HSGs and the length of the fiber shaft are involved in accumulation, in mouse and cynomolgus monkey liver, of systemically administered Ad vectors (Nakamura *et al.*, 2003; Smith *et al.*, 2003a,b; Vigne *et al.*, 2003).

Strategies to eliminate natural Ad tropism, based on modification of particular viral capsid proteins such as fiber and penton base (Wickham, 2000; Mizuguchi and Hayakawa, 2004), have been reported. To ablate CAR binding, Ad vectors containing an AB, DE, or FG loop mutation of the fiber knob (Bewley *et al.*, 1999; Kirby *et al.*, 1999; Alemany and Curiel, 2001; Einfeld *et al.*, 2001; Leissner *et al.*, 2001; Mizuguchi *et al.*, 2002; Smith *et al.*, 2002), Ad vectors containing the Ad type 40 short fiber (which has been hypothesized not to bind to any receptors; Nakamura *et al.*, 2003), and Ad vectors containing an external trimerization motif instead of the fiber knob (Hong *et al.*, 2003) have been developed. To ablate α_v integrin binding, Ad vectors with a deletion of the RGD (Arg-Gly-Asp) motif of the penton base (Einfeld *et al.*, 2001; Mizuguchi *et al.*, 2002; Vigne *et al.*, 2003) have been developed. To ablate HSG binding, Ad vectors mutated in the KKTK motif of the fiber shaft (Smith *et al.*, 2003b) have been developed.

Several groups have reported that Ad vectors from which CAR binding has been ablated do not change the biodistribution of Ad vectors (Alemany and Curiel, 2001; Leissner *et al.*, 2001; Mizuguchi *et al.*, 2002; Smith *et al.*, 2002), although Einfeld *et al.* have reported that CAR binding-ablated Ad vectors exhibit a 10-fold decrease in liver transduction (Einfeld *et al.*, 2001). Einfeld *et al.* have also reported that Ad vectors ablated for both CAR binding ablation and α_v integrin binding exhibit a more than 700-fold decrease in liver transduction (Einfeld *et al.*, 2001). Ad vectors ablated for α_v integrin binding, however, do not change their biodistribution (Mizuguchi *et al.*, 2002; Smith *et al.*, 2003b). Smith *et al.* have shown that HSG binding-ablated Ad vectors, in which the KKTK motif on the fiber shaft of Ad type 5 is changed to GAGA (Gly-Ala-Gly-Ala), exhibit a 15-fold decrease in liver transduction (Smith *et al.*, 2003b).

We have previously developed an Ad vector ablated for CAR, α_v integrin, and HSG binding by deleting four amino acids (T489, A490, Y491, and T492) from the FG loop of the fiber knob, deleting the RGD motif of the penton base, and substituting the fiber shaft domain for that derived from Ad type 35, which does not contain the HSG-binding motif (Koizumi *et al.*, 2003a). This triple-mutant Ad vector, on intravenous administration, showed more than 1000-fold lower gene transfer activity in mouse liver than the conventional Ad vector whereas double-mutant Ad vectors (ablated for CAR and α_v integrin binding, or for CAR and HSG binding), on intravenous administration, showed 100-fold lower gene transfer activity in mouse liver than the conventional Ad vector (Koizumi *et al.*, 2003a).

In the present study, we further improve the triple-mutant Ad vector by adding a mutation of the AB loop in the fiber knob (R412S, A415G, E416G, and K417G) instead of a deletion of the FG loop in the fiber knob. The AB loop in the fiber knob interacts directly with CAR and therefore must be the key anchor for the knob–CAR complex (Bewley *et al.*, 1999). In contrast, deletion of the FG loop in the fiber knob eliminates interactions between the fiber knob and CAR by changing the structure of the fiber knob (Kirby *et al.*, 1999). We examined in detail the gene transfer activity of the triple-mutant Ad vector containing a mutation of the AB loop in the fiber knob both *in vitro* and *in vivo* (intravenous and intraperitoneal administration) in comparison with the triple-mutant Ad vector containing a deletion of the FG loop in the fiber knob and the conventional Ad vector.

Another drawback of the Ad vector is the production (release) of cytokines and chemokines, as well as hepatotoxicity, after systemic injection of the vector (Lieber *et al.*, 1997; Liu *et al.*, 2003). The cytokines play a major causative role in liver damage associated with systemic Ad infusion as well as a role in the induction of an antiviral immune response. Cytokine production and release are thought to be the direct or indirect results of Ad uptake by Kupffer cells and their subsequent activation (Lieber *et al.*, 1997; Liu *et al.*, 2003) or lysis (Schiedner *et al.*, 2003). It is important to develop an Ad vector that reduces or blunts innate immune response. In the present study, we also show that systemic injection of the triple-mutant Ad vector does not increase serum interleukin (IL)-6 levels or liver serum enzymes (aspartate aminotransferase [AST] and alanine aminotransferase [ALT], which are hepatotoxicity marker enzymes).

MATERIALS AND METHODS

Cells

SK HEP-1 (endothelial cell line derived from human liver; Heffelfinger *et al.*, 1992) and 293 cells were cultured with Dulbecco's modified Eagle's medium (DMEM) supplemented with 10% fetal calf serum (FCS). Fiber-293 cells, which are stable transformants expressing Ad type 5 fiber protein (Koizumi *et al.*,

2003a), were cultured with DMEM supplemented with 10% FCS and hygromycin (GIBCO, 200 μg/ml; Invitrogen, Carlsbad, CA).

Plasmids and Ad vectors

The vector plasmid pAdHM59, which we used to generate Ad vectors containing a mutation of the AB loop of the fiber knob (R412S, A415G, E416G, and K417G), a deletion of the RGD motif in the penton base, and a substitution of the fiber shaft domain for that derived from Ad type 35, was constructed as follows. First, a polymerase chain reaction (PCR) fragment containing a sequence surrounding the AB loop of the Ad type 5 fiber knob gene (bp 32238–32495) was generated with primers (forward, 5′-ATTAATACTTTGTGGACCACACC-AGCTCCATCTCCTAACTGTAGcCTAAATGgAGgGggt-GATGCTAAACTCACTTTGGTCTTAACAAAA-3′ [the *Ase*I site is underlined and the mutation sequence is indicated by lower-case letters]; reverse, 5′-AGATCTCCATTTCTAAAG-TT-3′ [the *Bgl*II site is underlined]) and pGEM-Teasy-knob-CAR(+) as a template (Koizumi *et al.*, 2003a). The PCR fragment was then ligated with *Eco*RV-digested pcDNA3.1-Hygro (Invitrogen), resulting in pcDNA3.1-Hyg-AB4m. pcDNA3.1-Hyg-AB4mknob was constructed by three-piece ligation of (1) the *Afl*II/*Ase*I fragment of pF35-2.3(AseI) (Mizuguchi and Hayakawa, 2002), which contains the fiber shaft of Ad type 35, (2) the *Ase*I/*Bgl*II fragment of pcDNA3.1-Hyg-AB4m, and (3) the *Afl*II/*Bgl*II fragment of pcDNA3.1-Hygro. Next, pHM-S35-K5-AB4m was constructed by three-piece ligation of (1) the *Afl*II/*Bgl*II fragment of pcDNA3.1-Hyg-AB4mknob, (2) the *Mun*I/*Bgl*II fragment of pHM-S35-K5-CAR(+) (Koizumi *et al.*, 2003a), and (3) the *Afl*II/*Mun*I fragment of pHMCMV6 (Mizuguchi and Kay, 1999). pHM-S35-K5-AB4m contains the sequence encoding the CAR-binding ablated Ad type 5 fiber knob (mutation of the sequence encoding four amino acids in the AB loop), a *Csp*45I site in the HI loop, a *Cla*I site in the C-terminal end of the fiber knob-coding sequence, and the fiber shaft sequence of Ad type 35. pS35-K5-2.2-AB4m was then constructed by ligation of *Srf*I/*Mun*I-digested pHM14-Eco2 (Koizumi *et al.*, 2003b) and *Srf*I/*Mun*I-digested pHM-S35-K5-AB4m. Next, the *Srf*I/*Mun*I fragment of pS35-K5-2.2-AB4m was ligated with the *Srf*I/*Mun*I fragment of pHM14-Eco12, resulting in the creation of pHM14-Eco2-S35-AB4m, which contains the Ad genome from bp 27331 to the end of the Ad genome and contains the sequence encoding the substitution of the fiber shaft domain for that derived from Ad type 35 and the mutation of the AB loop of the fiber knob. Finally, pAdHM59 was constructed by ligation of *Eco*RI/*Cla*I-digested pHM14-Eco2-S35-AB4m (the location of the *Eco*RI site is bp 27332 in the Ad genome, whereas the *Cla*I site is in the C-terminal end of the fiber-coding sequence) and *Eco*RI/*Cla*I-digested pAdHM43 (Koizumi *et al.*, 2003a), which contains the complete Ad genome, deletion of the RGD motif in the penton base, and a *Cla*I site in the C-terminal end of the fiber-coding sequence. pAdHM59 has a complete E1/E3-deleted Ad genome with I-*Ceu*I, *Swa*I, and PI-*Sce*I sites in the E1 deletion region, *Pac*I sites at both ends of the Ad genome, and deletion of the RGD peptide-coding sequence of the penton base (MND-HAIRGDTFATRAE was changed to MNDTSRAE), and contains the chimeric fiber-coding sequence of the CAR binding-ablated Ad type 5 fiber knob (mutation of the AB loop-coding region of the fiber knob [R412S, A415G, E416G, and K417G]), the Ad type 35 fiber shaft sequences, and the Ad type 5 fiber tail sequence. pAdHM59 also contains a unique *Csp*45I site in the HI loop of the fiber knob-coding sequence and a *Cla*I site in the C-terminal end of the fiber knob-coding sequence. Therefore, the targeting ligands can be easily displayed in the fiber knob of the vectors by cloning the respective genes into these regions by simple *in vitro* ligation.

Ad vectors were constructed by an improved *in vitro* ligation method described previously (Mizuguchi and Kay, 1998, 1999). pAdHM59-CMVL2 and pAdHM54-CMVL2 were constructed by ligation of I-*Ceu*I/PI-*Sce*I-digested pAdHM59 and pAdHM54, respectively, and I-*Ceu*I/PI-*Sce*I-digested pCMVL1 (Mizuguchi and Kay, 1999). To construct pAdHM59-RGD-CMVL2, pAdHM59 was first digested with *Csp*45I and ligated with oligonucleotide 1 (5′-cggcctgtgactgccgcggagactgtttctgc-gatg-3′) and oligonucleotide 2 (5′-cgcatcgcagaaacagtctccgcg-gcagtcacaggc-3′), which corresponds to the RGD (RGD-4C) peptide, CDCRGDCFC, with high affinities for integrins ($\alpha_v\beta_3$ and $\alpha_v\beta_5$) (Koivunen *et al.*, 1995; Pasqualini *et al.*, 1997), resulting in the creation of pAdHM59-RGD. I-*Ceu*I/PI-*Sce*I-digested pAdHM59-RGD was then ligated with I-*Ceu*I/PI-*Sce*I-digested pCMVL1, resulting in the creation of pAdHM59-RGD-CMVL2.

To generate the virus, pAdHM59-CMVL2, pAdHM54-CMVL2, and pAdHM59-RGD-CMVL2 were digested with *Pac*I and purified by phenol–chloroform extraction and ethanol precipitation. Linearized DNAs were transfected into Fiber-293 cells (in the case of pAdHM54-CMVL2 and pAdHM59-CMVL2) or 293 cells (in the case of pAdHM59-RGD-CMVL2) with Super-Fect (Qiagen, Valencia, CA) according to the manufacturer's instructions. When pAdHM59-CMVL2 and pAdHM54-CMVL2 were transfected into normal 293 cells, the virus was not generated because the virus does not interact with 293 cellular receptors. Viruses [Ad/ΔF(AB)ΔP-S35-L2, Ad/ΔF(FG)ΔP-S35-L2, and Ad/ΔF(AB)ΔP-S35-RGD-L2] were prepared by standard methods with the exception that Ad/ΔF(AB)ΔP-S35-L2 and Ad/ΔF(FG)ΔP-S35-L2 were amplified with Fiber-293 cells, and that only the last step of viral amplification was performed by infection into normal 293 cells, as described previously (Koizumi *et al.*, 2003a). Ad/ΔF(FG)ΔP-S35-L2 is identical to Ad/ΔFΔP-S35-L2 in our previous report (Koizumi *et al.*, 2003a). A conventional luciferase-expressing Ad vector, Ad-L2, had been constructed previously (Mizuguchi and Kay, 1999). Viruses were purified by $CsCl_2$ step gradient ultracentrifugation followed by $CsCl_2$ linear gradient ultracentrifugation. Determination of virus particle titers was accomplished spectrophotometrically by the methods of Maizel *et al.* (1968). Virus particle titers of the vector stocks, prepared from five 150-mm dishes (approximately 8×10^7 cells), were as follows: Ad-L2, 1.8×10^{12} vector particles (VP)/ml; Ad/ΔF(AB)ΔP-S35-L2, 2.8×10^{12} VP/ml; Ad/ΔF(FG)ΔP-S35-L2, 3.3×10^{12} VP/ml; Ad/ΔF(AB)ΔP-S35-RGD-L2, 2.6×10^{12} VP/ml.

Western blotting

Five hundred nanograms of virus in 1× sample buffer containing 4% 2-mercaptoethanol was loaded onto a sodium dodecyl sulfate (SDS)–polyacrylamide gel after boiling for 5 min, followed by electrotransfer to a nitrocellulose membrane. After blocking in Block Ace (Dainippon Pharmaceutical, Osaka, Japan), the filters were incubated with a rabbit fiber knob polyclonal antibody (diluted 1:3000) (kindly provided by R.D. Gerard, University of

Texas Southwestern Medical Center, Dallas, TX), followed by incubation in the presence of peroxidase-labeled anti-rabbit antibody (diluted 1:10,000) (Cell Signaling Technology, Beverly, MA). The filters were developed by chemiluminescence (ECL Western blotting detection system; GE Healthcare, Little Chalfont, UK), and signals were read with an LAS-3000 imaging system (Fujifilm Medical Systems USA, Stamford, CT).

Adenovirus-mediated gene transduction into cultured cells

SK HEP-1 cells (1×10^4 cells) were seeded in a 96-well dish. On the next day, they were transduced with Ad-L2, Ad/ΔF(FG)ΔP-S35-L2, Ad/ΔF(AB)ΔP-S35-L2, or Ad/ΔF(AB)ΔP-S35-RGD-L2 (3000 VP/cell) for 1.5 hr. After a 48-hr culture period, luciferase production in the cells was measured with a luciferase assay system (PicaGene LT2.0 luminescence kit; Toyo Ink, Tokyo, Japan).

In the experiment to quantify Ad uptake into SK HEP-1 cells, the cells were incubated at 37°C for 1.5 hr with the corresponding virus, washed with phosphate-buffered saline (PBS), resuspended in 0.05% trypsin–0.5 m*M* EDTA-PBS solution, and incubated at 37°C for 10 min. After this incubation, the cells were incubated at 37°C for 10 min with 0.05% DNase I–0.5 *M* $MgCl_2$–PBS, washed with PBS, and resuspended in 0.1 *M* EDTA–PBS solution. Finally, the Ad genome DNA in the cells was quantified with a TaqMan fluorogenic detection system (ABI PRISM 7700 sequence detector; Applied Biosystems, Foster City, CA). Sample DNA was isolated with an automatic nucleic acid isolation system (NA-2000; Kurabo Industries, Osaka, Japan). The Ad vector DNA standard was pAdHM4 plasmid DNA (Mizuguchi and Kay, 1999). Primers for amplification were located in the E4 region, with the sequences CACCACCTCCCGGTACCATA (sense) and CCGCACCTGGTTTTGCTT (antisense). The fluorogenic detection probe had the sequence AACCTGCCCGCCGGCTATACACTG. Samples were amplified in 50 μl for 40 cycles in the ABI PRISM 7700 sequence detector with continuous fluorescence monitoring. Data were processed with ABI PRISM 7000 SD software (Applied Biosystems).

When SK HEP-1 cells were transfected with a complex of Ad/ΔF(AB)ΔP-S35-L2 and SuperFect (Qiagen), the cells (2×10^4 cells) were seeded in a 48-well dish. The next day, the cells were transduced with Ad/ΔF(AB)ΔP-S35-L2 (10,000 VP/cell) in the presence of SuperFect (0, 0.15, or 1.5 μg; Qiagen) for 1.5 hr. After a 48-hr culture period, luciferase production in the cells was measured with a luciferase assay system (PicaGene PGL5500; Toyo Ink).

In the competition experiments, SK HEP-1 cells (2×10^4 cells) were seeded in a 48-well dish. The next day, the cells were preincubated with RGD peptide (GRGDSP; TaKaRa, Osaka, Japan) (0, 40, or 200 μg/ml) for 10 min at room temperature. The cells were then transduced with Ad/ΔF(AB)ΔP-S35-RGD-L2 (300 VP/cell) for 0.5 hr. After 48 hr in culture, luciferase production in the cells was measured by luminescence assay (PicaGene LT2.0; Toyo Ink).

Adenovirus-mediated gene transduction in vivo

Ad-L2, Ad/ΔF(FG)ΔP-S35-L2, Ad/ΔF(AB)ΔP-S35-L2, or Ad/ΔF(AB)ΔP-S35-RGD-L2 was intravenously (3.0×10^{10} VP) or intraperitoneally (1.0×10^{11} VP) administered to C57BL/6 mice (male, 5 weeks old; obtained from Nippon SLC, Shizuoka, Japan). Forty-eight hours later, the heart, lung, liver, kidney, and spleen were isolated and homogenized as previously described (Xu *et al.*, 2001). Luciferase production was determined with a luciferase assay system (PicaGene 5500; Toyo Ink). Protein content was measured with a Bio-Rad assay kit (Bio-Rad, Hercules, CA), using bovine serum albumin as a standard.

The amounts of Ad genomic DNA in each organ were quantified with the TaqMan fluorogenic detection system (ABI PRISM 7700 sequence detector; Applied Biosystems). Samples were prepared with isolated DNA templates from each organ (25 ng) by the automatic nucleic acid isolation system (NA-2000; Kurabo Industries). The amounts of Ad DNA were quantified with the TaqMan fluorogenic detection system (Applied Biosystems), as described above.

Amounts of Ad vector DNA in liver parenchymal and nonparenchymal cells

Ad-L2, Ad/ΔF(FG)ΔP-S35-L2, or Ad/ΔF(AB)ΔP-S35-L2 was intravenously (3.0×10^{10} VP) or intraperitoneally (1.0×10^{11} VP) administered to C57BL/6 mice (male, 5 weeks old; Nippon SLC). Mice were anesthetized by intraperitoneal administration of pentobarbital sodium (Dainippon Pharmaceutical) 3 hr after Ad vector injection. Liver cells were separated into parenchymal cells (PCs; hepatocytes) and nonparenchymal cells (NPCs) (Kupffer cells and endothelial cells), as described previously (Nishikawa *et al.*, 1998). Briefly, the liver was perfused with HEPES buffer (pH 7.5) containing collagenase. The dispersed cells were separated into PC and NPC fractions by differential centrifugation. Quantitative PCR was performed to examine the amounts of Ad vector DNA in the PCs and NPCs. Total DNA, including the Ad vector DNA, was isolated from the PCs and NPCs by means of the automatic nucleic acid isolation system (NA-2000; Kurabo Industries). The amounts of Ad DNA were quantified with the TaqMan fluorogenic detection system (Applied Biosystems), as described above.

Blood clearance of Ad vectors

Blood samples were collected by retroorbital bleeding at the indicated times (2, 10, and 30 min; or 2, 60, 120, and 180 min) after intravenous (3.0×10^{10} VP) or intraperitoneal (1.0×10^{11} VP) administration of Ad-L2, Ad/ΔF(FG)ΔP-S35-L2, or Ad/ΔF(AB)ΔP-S35-L2. Total DNA, including the Ad vector DNA, was isolated from whole blood with a QIAamp DNA blood mini kit (Qiagen). The amounts of Ad DNA were quantified with the TaqMan fluorogenic detection system (Applied Biosystems), as described above.

Liver serum enzymes and interleukin-6 levels after systemic administration

Blood samples were collected from the inferior vena cava at the indicated times (3 or 48 hr) after intravenous (3.0×10^{11} VP) or intraperitoneal (1.0×10^{11} VP) administration of Ad-L2, Ad/ΔF(AB)ΔP-S35-L2 or Ad/ΔF(FG)ΔP-S35-L2. Serum samples were collected into separate tubes containing no anticoagulant for coagulation. The levels of AST and ALT in serum samples collected at 48 hr were measured with a Transaminase-CII kit (Wako Pure Chemical Industries, Osaka, Japan). IL-6 levels in serum samples collected 3 hr after Ad injection were

measured with an enzyme-linked immunosorbent assay (ELISA) kit (BioSource International, Camarillo, CA).

RESULTS

Construction of vectors that abolish natural viral tropism is the first step in the development of targeted Ad vectors. Identification and incorporation of a foreign ligand with high affinity for a specific cellular receptor into the capsid of Ad vectors that no longer infect cells would be the next step (Fig. 1A). This study was undertaken to improve a previously developed triple-mutant Ad vector that no longer infects cells by deletion of the FG loop of the fiber knob, deletion of the RGD motif of the penton base, and substitution of the fiber shaft domain with that derived from Ad type 35. Hepatocyte toxicity and innate immune response (IL-6 production) by systemic injection of the vectors were also examined.

Generation of several types of mutant Ad vector

To examine the effects of the various fiber knob mutations (mutation of AB loop or deletion of FG loop) in the triple-mutant Ad vector on gene transfer activity *in vitro* and *in vivo*, we constructed several types of mutant Ad vector expressing luciferase. Ad/ΔF(AB)ΔP-S35-L2 contains the Ad type 5 fiber knob

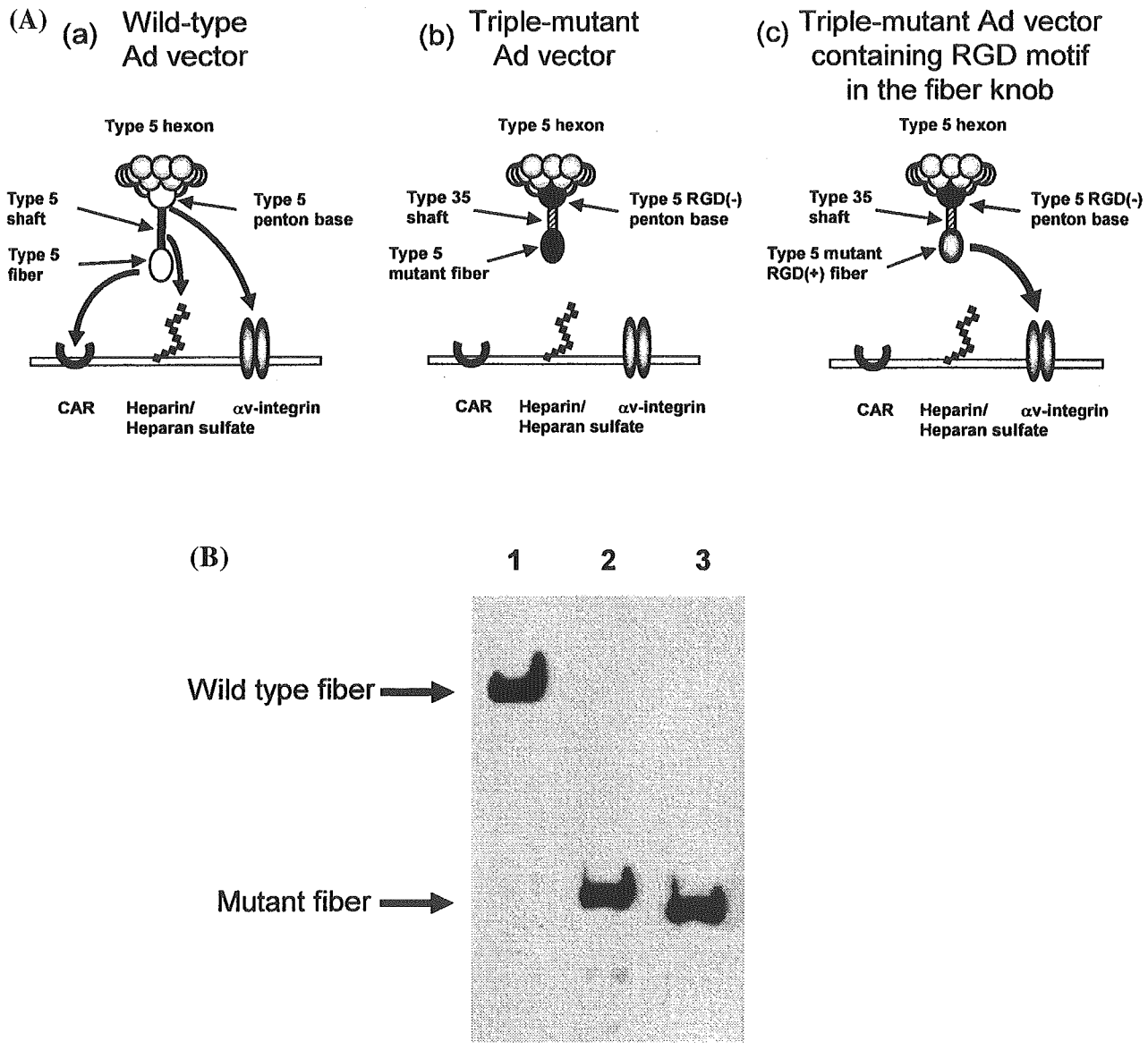

FIG. 1. Mutant Ad vectors. (**A**) Schematic diagram of the interaction of mutant Ad vectors with cells. The wild-type Ad vector infects cells by interactions of the fiber knob with CAR, the fiber shaft with HSGs, and the penton base with α_v integrin. The triple-mutant Ad vector does not have these interactions with cells. The triple-mutant Ad vector containing the RGD motif in the HI loop of the fiber knob infects cells via interaction of the RGD motif with α_v integrin. (**B**) Western blot analysis of the fiber protein in Ad-L2, Ad/ΔF(FG)ΔP-S35-L2, and Ad/ΔF(AB)ΔP-S35-L2. Five hundred nanograms of virus was separated on a 12% SDS–polyacrylamide gel, and the fiber protein was analyzed by Western blotting using a rabbit fiber knob polyclonal antibody as described in Materials and Methods. Lane 1, Ad-L2; lane 2, Ad/ΔF(FG)ΔP-S35-L2; lane 3, Ad/ΔF(AB)ΔP-S35-L2.

TABLE 1. ADENOVIRAL VECTOR MUTATIONS AND POTENTIAL CELL INTERACTIONS

Ad vector	*Amino acid sequence of knob domain*				*Type of Ad shaft*	*Type of Ad tail*	*Penton base*	*Type of Ad vector*[a]
	AB loop	*FG loop*	*HI loop*	*C terminus*				
Conventional Ad								
Ad-L2	–NCRLNAEKDA–	–TEGTAYTNAV–	–DTTPSA–	–QE stop	5 (22 β repeats)	5	MND–HAIRGDTFAT–RAE	a
Triple-mutant Ads								
Ad/ΔF(FG) ΔP-S35-L2	–NCRLNAEKDA–	–TEG----NAV– (Δa.a. 489–492)	–DTTSNPSA–	–QEID stop	35 (6 β repeats)	5	MND–TS----------RAE ΔRGD motif	b
Ad/ΔF(AB) ΔP-S35-L2	–NCSLNGGGDA– (4-a.a. mutation)	–TEGTAYTNAV–	–DTTSNPSA–	–QEID stop	35 (6 β repeats)	5	MND–TS----------RAE ΔRGD motif	b
Triple-mutant Ad containing RGD motif in fiber								
Ad/ΔF(AB) ΔP-S35-RGD-L2	–NCSLNGGGDA– (4-a.a. mutation)	–TEGTAYTNAV–	–DTTSACDCRG DCFCANPSA–	–QEID stop	35 (6 β repeats)	5	MND–TS----------RAE ΔRGD motif	c

[a]See Fig. 1A.